Naval Research Reviews

Office of Naval Research
One / 1991
Vol XLIII

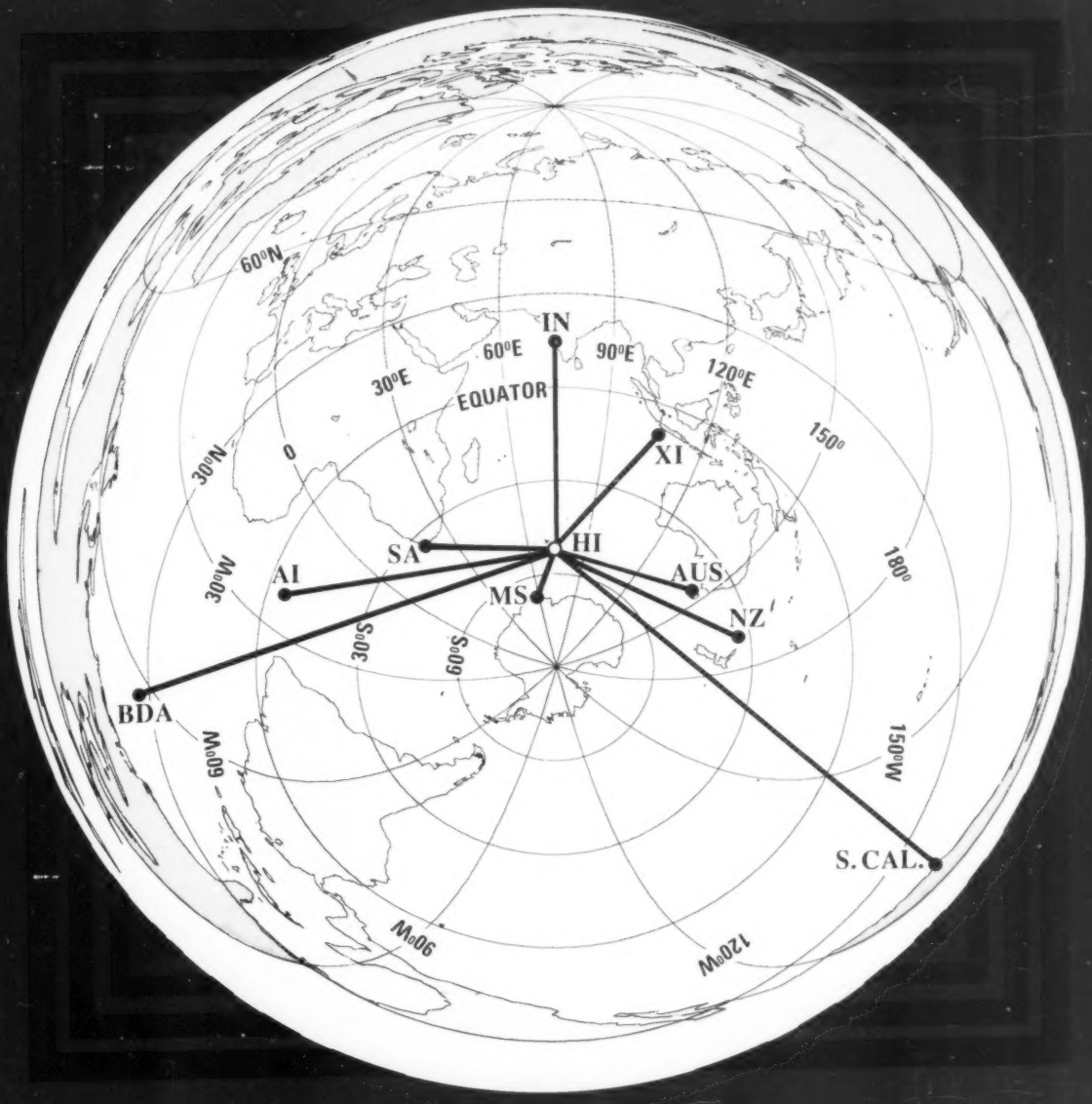

Inflatoplane Takes Off

This eccentric plane from the annals of aerodynamics might be called aviation trivia but it did fly. The Office of Naval Research (ONR) started the inflatoplane project in 1956 and a year later it took flight. The inflatable rubber aircraft manufactured by Goodyear Aircraft Corporation for ONR featured an enclosed cockpit, one-piece wing and simplified controls. The wing, tail assembly and cockpit were made of airmate (two walls of rubberized fabric connected by nylon threads). An air hose or household vacuum cleaner was used to pump up the inflatoplane. The craft was made rigid with less air pressure than that required to inflate a tire on the family car. It was powered by a 44 horsepower Nelson engine. The plane was outfitted with a hydro-ski of a lightweight aluminum alloy for operating on water. The ski could be attached to the landing gear in a matter of minutes.

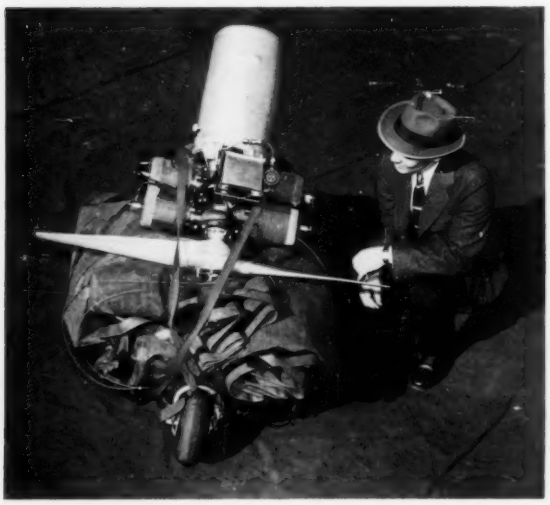

The folded up inflatoplane package

The spread out inflatoplane ready for inflation

Naval Research Reviews

Office of Naval Research
One / 1991
Vol XLIII

Articles

2
The Heard Island Experiment
by Walter H. Munk

30
Development of a Planar Fiber Optic Hydrophone for Measuring the Low Wavenumber Pressure Components of Turbulent Boundary Layers
by P. C. Shang
P. J. Zoccola
S. A. Fisher
Y. F. Hwang

24
Results of an Efficient Gating Algorithm for Large-Scale Tracking Scenarios
by Jeffrey K. Ulhmann
Miguel R. Zuniga

Departments

23
Profiles in Science

40
Research Notes

CHIEF OF NAVAL RESEARCH
RADM William C. Miller, USN

DIRECTOR
Dr. Fred Saalfeld

CHIEF WRITER/EDITOR
William J. Lescure

SCIENTIFIC EDITORS
Dr. Robert J. Nowak
Dr. J. Dale Bultman
Sarah Scott

MANAGING EDITOR
Norma Gerbozy

ART DIRECTION
Typography and Design
Desktop Printer, Arnold, MD

About the Cover

The Heard Island Experiment is designed to assess the feasibility of global ocean warming measurement by long-range sound propagation. On January 26, 1991 low frequency (57 Hz) coded signals were transmitted from Heard Island to an international coalition of listening stations in or near Antarctica (MS), South Africa (SA), Australia (AUS), Christmas Island (XI), India (IN), Ascension Island (AI), Monterey California (S. CAL.), Bermuda (BDA), Hawaii (HI), a New Zealand ship in the Tasman Sea (AUS), and a Canadian ship off the U.S. East Coast (BDA). (See article on page 2.)

Naval Research Reviews publishes articles about research conducted by the laboratories and contractors of the Office of Naval Research and describes important naval experimental activities. Manuscripts submitted for publication, correspondence concerning prospective articles, and changes of address, should be directed to Code OPARI, Office of Naval Research, Arlington, VA 22217-5000. Requests for subscriptions should be directed to the Superintendent of Documents, U.S. Government Printing Office, Washington, DC 20403. *Naval Research Reviews* is published from appropriated funds by authority of the Office of Naval Research in accordance with Navy Publications and Printing Regulations. NAVSO P-35.

The Heard Island Experiment

Walter H. Munk
Scripps Institution of Oceanography

Preface:

The International Sciences Lecture Series

At the request of the Office of Naval Research the International Science Lecture Series was established in mid-1990 as a joint endeavor with the National Academy of Sciences-National Research Council for the expressed purpose of advancing communication and cooperation within the international scientific community. A search committee established by the National Research Council is charged with selecting two prominent American scientists each year (beginning in 1991)to lecture on the latest research results in areas of scientific inquiry pre-selected by the two sponsors. The countries in which the lectures are to be given are worked out in consultation with representatives of the international scientific community, with the science attaché in the relevant American embassies, and with senior representatives of Office of Naval Research-Asia and Office of Naval Research-Europe. Wherever appropriate, each lecture is followed by formal and informal discussions with senior representatives of the scientific community in the host country to expand the dialogue on research progress, problems, and plans of common interest. Following each tour, the lecture will be published for wider international distribution.

The inaugural lecture in the series was presented during November 1990 by Professor Walter Munk of the Scripps Institution of Oceanography. Professor Munk lectured on the planned "Heard Island Experiment" – a ten-year research program aimed at monitoring global warming by measuring ocean temperature changes as a function of acoustic travel times across the Atlantic, Pacific, and Indian ocean basins from a sound source near Heard Island in the southern Indian Ocean. A ten day feasibility test was carried out at Heard Island during January. The success of this test warranted proceeding with the ten year plan and the data received is now being analyzed.

Accompanied on the tour by Bernard J. Zahuranec of the Office of Naval Research, and Lee M. Hunt of the National Research Council, Professor Munk presented the lecture in Paris, France; in Cochin, Goa, Delhi, and Ahmedabad, India; and in Jakarta, Indonesia. In Paris the lecture was sponsored by the French Academy of Sciences. In Cochin it was presented before the annual meeting of the Indian Acoustical Society, and at the Naval Physical and Oceanographic Laboratory. In Goa the lecture was given at the National Institute of Oceanography. In Delhi the lecture was sponsored by the Indian Academy of Sciences, and as the first of a Distinguished Lecture Series sponsored by the Department of Ocean Development. The lecture was given at the National Physical Laboratory. The final lecture in India was presented at the Physical Research Laboratory in Ahmadabad. In Jakarta the lecture was presented before an audience at the Indonesian Agency for the Application and Assessment of Technology. Both Professor Munk and the lecture were received with interest and enthusiasm at each of the above locations, and the formal and informal discussions that followed were well attended and revealed many areas of common interest in oceanographic research.

The sponsors would like to acknowledge the invaluable assistance of the many individuals in France, India, and Indonesia who made the inaugural lecture of the International Science Lecture Series a success. Prominent among these are Dr. James Andrews, Chief Scientist of ONR-Europe; Dr. Willem H. Brakel and Dr. Michael Michaud of the Science and

Figure 1

The Keeling time series of CO_2 concentration at Mauna Loa.[1]

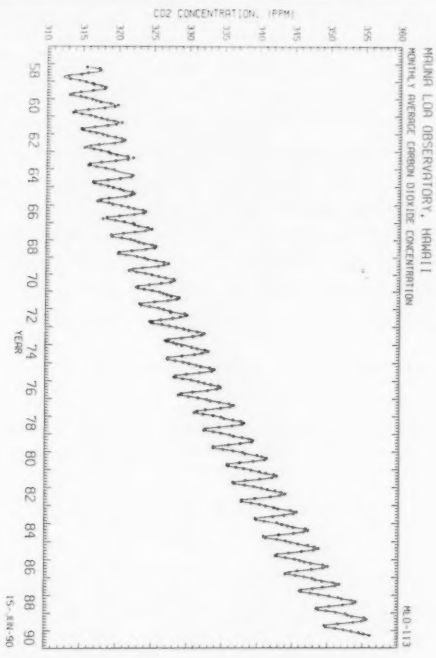

Figure 2

An extension of the Keeling annual means back to 1740, using measurements made on Antarctic ice cores.[2]

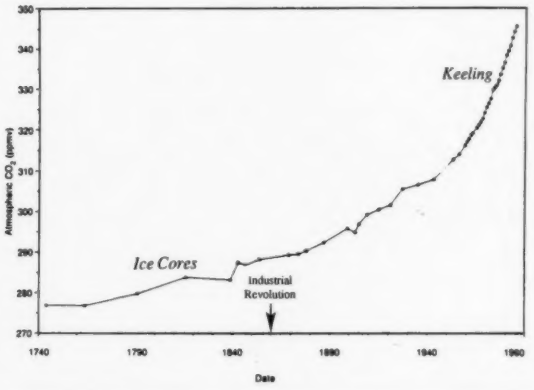

Technology Affairs Office of the American Embassy in Paris; Dr. P.L.M. Heydemann, Dr. S.K. Dutt, Ms. Sundari Kumar, and Ms. Lakshmi Kinger of the American Embassy in Delhi; and Dr. Jeffrey T. Lutz and Ms. Kemala Angraini Ahwil of the American Embassy in Jakarta for both arrangements and participation in meetings. Dr. Sach Yamamoto, Chief Scientist of ONR-Asia and Dr. David Evans of the ONR Washington Office also provided valuable assistance.

The sponsors would also like to thank their scientific colleagues in all three countries for their warm hospitality, and for the many arrangements: Dr. Claude Jablon (French Academy of Sciences) and Dr. Klaus Voigt (Deputy Secretary, Intergovernmental Oceanographic Commission); Dr. V.K. Aatre (Director, Naval Physical and Oceanographic Labora-

TABLE 1. Parameters

INDUSTRIAL REVOLUTION

	1860	1990	Δ
CO_2	280	355	+75 ppm
Surface Flux	238	240	+2 W/m^2
T (equilibrium)	15°C	16°C	+1° C
T (measured)	15°C	15.5°C	+0.5° C

1990 CO_2 BUDGET (GTC/year)

SOURCES		SINKS	
FUEL	5.7	ATMOSPHERE	3.7
FORESTS	1.8	BIOSPHERE	2.1
METHANE	0.5	OCEANS	2.2
	8.0		8.0

1990 WARMING (m°C/year)

T_{ATM} (equilibrium)	32	
T_{ATM} (measured)	20	~~~→ 0.03 W/m^2
T_{OCEAN} (surface)	20	~~~→ 1.7 W/m^2
T_{OCEAN} (1 km depth)	4	1.8 mm/year

tory), Dr. B.N. Desai (Director, National Institute of Oceanography), Dr. S.K. Joshi (Director, National Physical Laboratory, and Foreign Secretary, Indian Academy of Sciences), Dr. V.K. Gaur (Secretary, Department of Ocean Development), Dr. A.P. Mitra (Director General, Council of Scientific and Industrial Research), Dr. V.R. Gowariker (Secretary, Department of Science and Technology); and Dr. IR.H. Wiryosumarto (Bidang Pengembangan Teknologi).

The Experiment

The Director of Office of Naval Research is routing me around the world to talk of an experiment to take place. This is a risky mission, like playing the futures. I would much rather be talking here next year about what we have learned.

Atmospheric CO_2

Keeling's three decades of painstaking CO_2 measurements at Mauna Loa Observatory (figure 1) have played a major role in an ongoing debate on global energy policy.[1] I wish to raise two issues. First, that no one would today question the value of Keeling's research program. Yet, support for the program was not so readily forthcoming when Revelle and Suess proposed that an important increase in atmospheric CO_2 was taking place even then, in 1956, at a rate measurable with then available techniques. The theme of my talk is that the upper kilometer of ocean may be warming even now, in 1990, at a rate measurable with available techniques.

Second, why does no one question the existence of the CO_2 trend? Because the time series is of sufficient length for the long-term trend to equal 40 sigma (standard deviations). To detect a trend in a noise at the 95% level takes time enough

Figure 3

The Hansen time series of global average surface temperature[3] (left top) and the MacDonald decomposition[4] into an ambient low frequency component (left bottom) and a trend plus high frequencies (right bottom). The reference frequency is 4 cycles per century (right top).

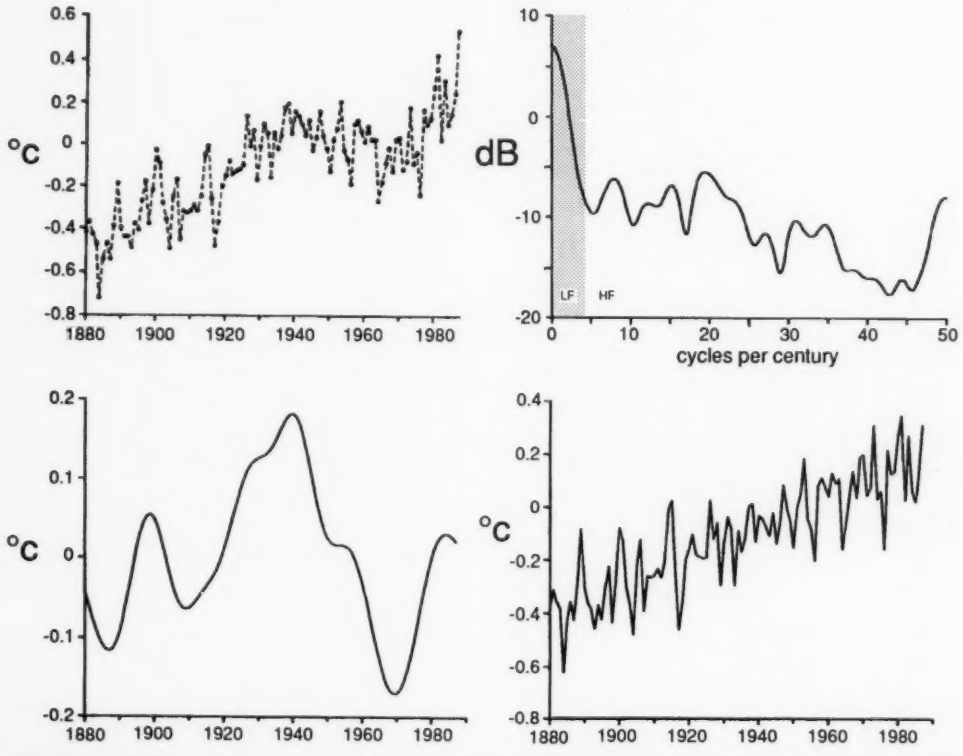

Figure 4

Three detonations in the sound channel off Perth were clearly recorded on Bermuda hydrophones half-way around the Earth.[7,8]

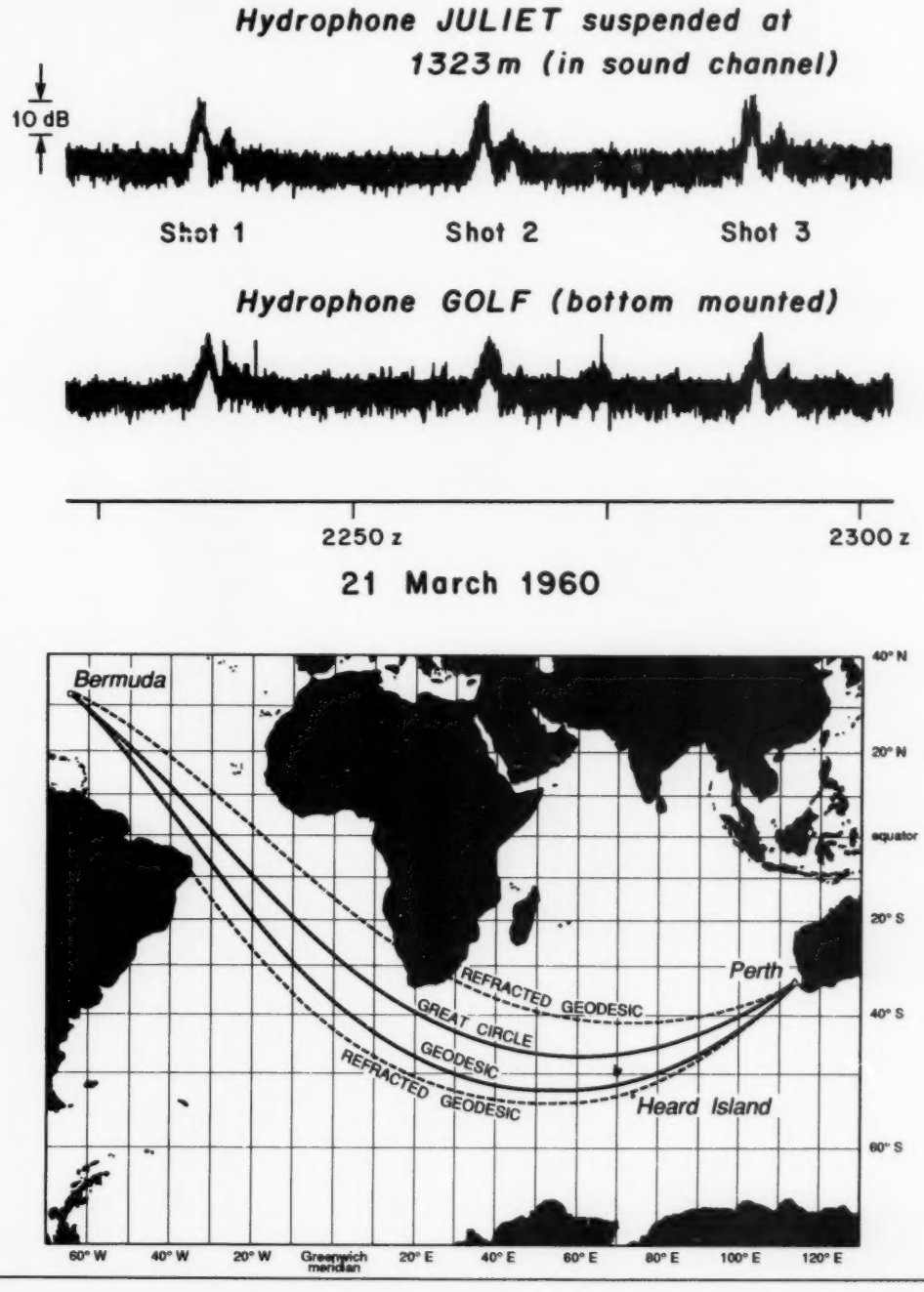

Figure 5

Observations used by Reid [8] to compute the global sound channel.

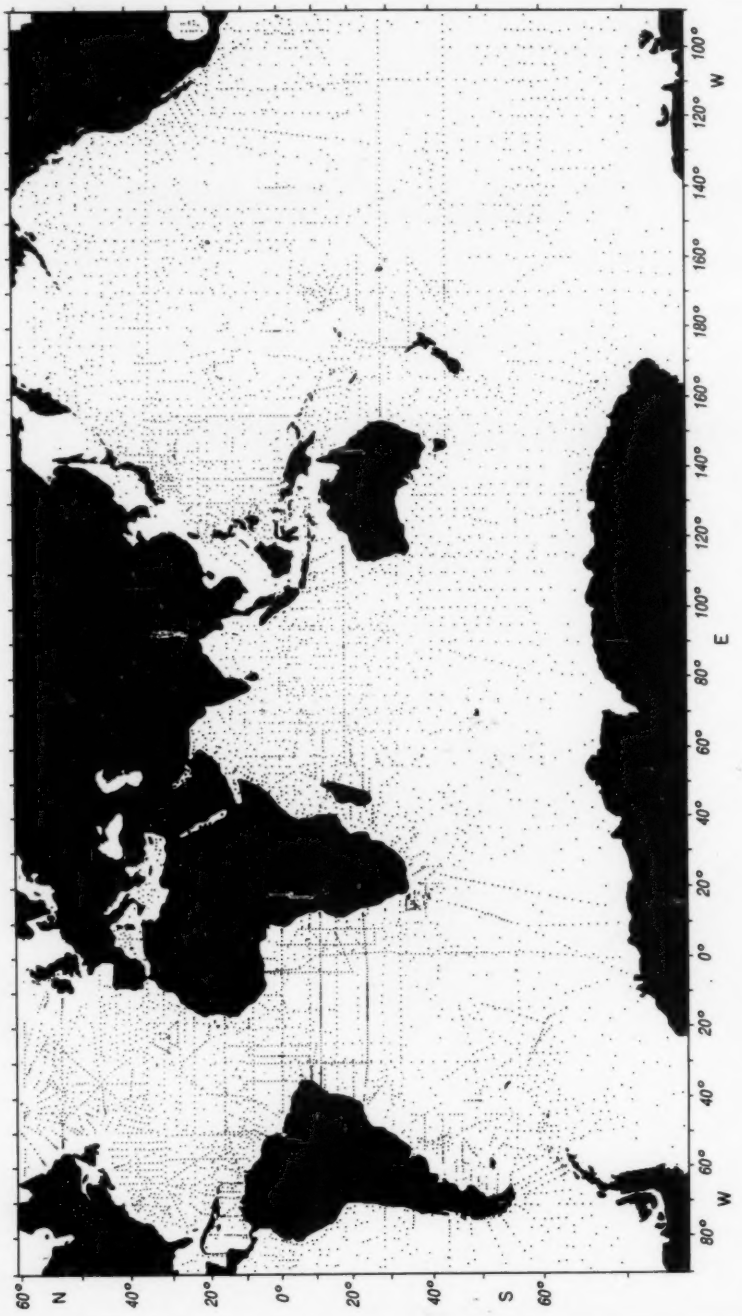

for the trend to reach 4 sigma (under certain assumptions), or 5 years for the CO_2 record. (Most of the variance here is due to seasonal variability; the situation can be much more complicated for a continuous variance spectrum.)

Keeling's measurements started in 1958. Antarctic ice cores have made it possible to reconstruct CO_2 history back to 1740, with a good match to Keeling (figure 2).[2] Zero time is taken for the industrial revolution in 1860 with 280 ppm of

Figure 6

Depth (m) and sound speed (m/s) at the sound channel.[8]

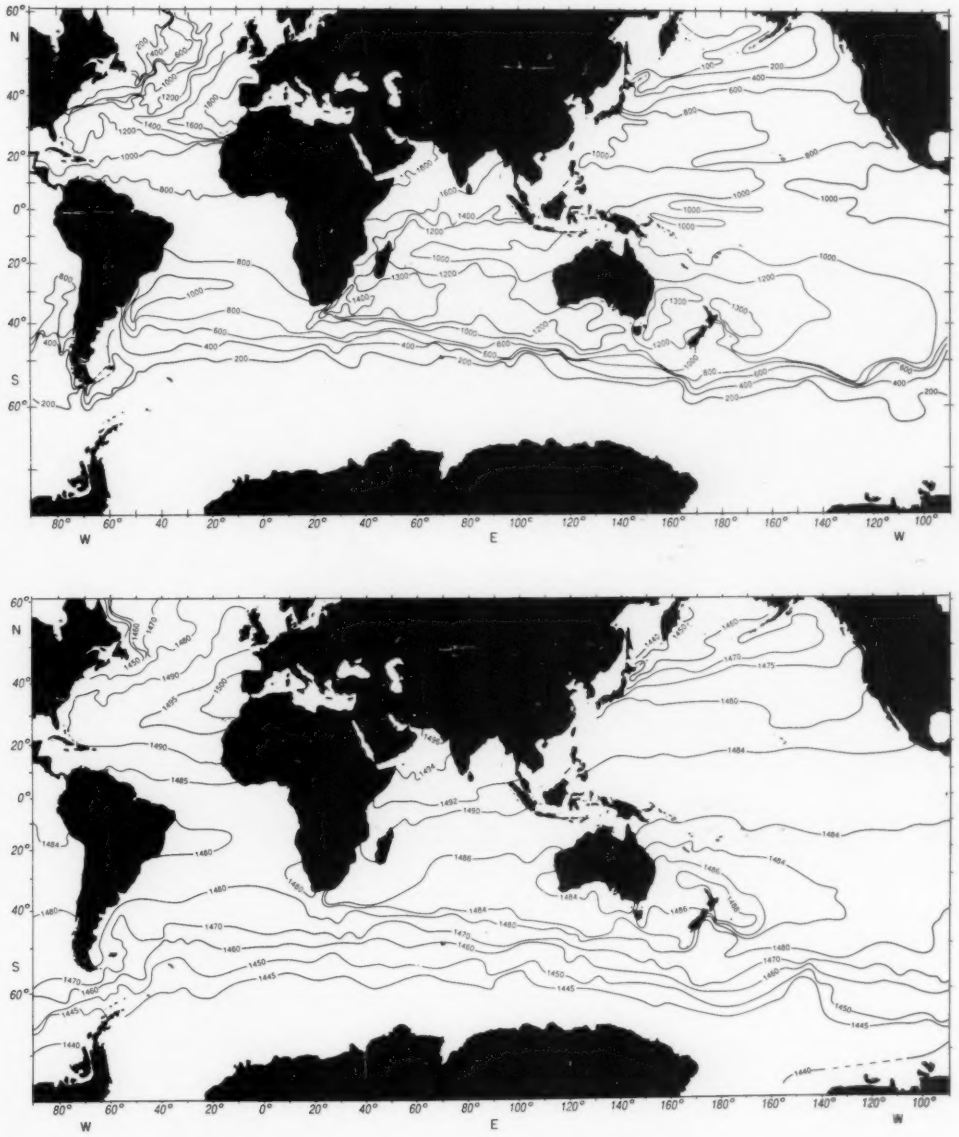

Figure 7

Axially refracted geodesics drawn every 10° from the source location at Heard Island.[9] Receiver sites are shown. Horizontal lines represent horizontal arrays off the American west coast and off Bermuda. Vertical lines designate vertical arrays off Monterey and Bermuda. Lines with arrow designate a Canadian towed array off British Columbia and a New Zealand towed array. The Japanese will occupy a station near Fiji Island. The Australians (our principal partners) will occupy three stations, one near Christmas Island in the Indian Ocean, one off Tasmania and a third at Mawson Station, Antarctica. There will be a French receiver east of Kerguelen Island, an Indian receiver off Goa, and a station by the University of Cape Town. NOAA will record axial receivers at Ascension Island. A USSR acoustic vessel will record at 25°N in the North Atlantic. There may be a station off Brazil. An attempt will be made to record the signal on land with a high-frequency seismic array on Ascension Island, and possibly in the Tahitian area.

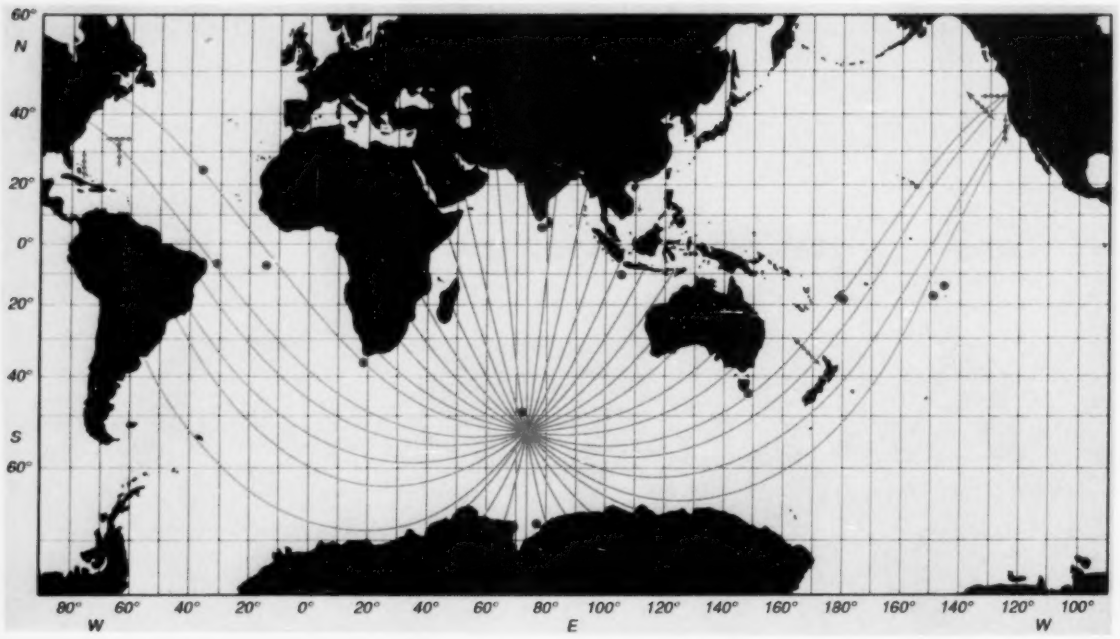

CO_2. The increase has been by a very respectable 27%. There have been many attempts to reconcile the 27% increase with global fuel consumption. A budget estimate for 1990 is given in table 1. Radiation reaching the outer atmosphere equals 1333 W/m^2(solar constant), of which 280 W/m^2 gets to the surface. Given the increases in greenhouse gases since 1860, various investigators have computed the associated increase in surface heat flux to be about 2 W/m^2, and the resulting increase in equilibrium surface temperature to be about 1°C. We will show next that the *measured* increase is by only 0.5°C; the difference is attributed to ocean heat storage. The ocean is also a significant sink of CO_2 (the oceanic 2.2 gigatons of carbon per year are based on balancing the budget, not (as yet) on direct measurements. Without ocean heat storage the atmospheric temperature increase 1860-1990 would be 1°C instead of 0.5°C; without ocean CO_2 storage, it would be up 1.6°C instead of 0.5°C. So the oceans are an important sink for greenhouse gases and an important sink for heat (as well as a sink for ignorance since the ocean changes are not measured but inferred).

Atmospheric Temperature.

The reconstruction of global temperature increase over the last 108 years by Hansen and Lebedeff[3] gives 0.5°C, one half the equilibrium warming. There are many difficulties in deriving this estimate (see figure 3).[3,4] The distribution is biased in favor of northern hemisphere land stations. Many of

Figure 8

The acoustic source is shown to the right.

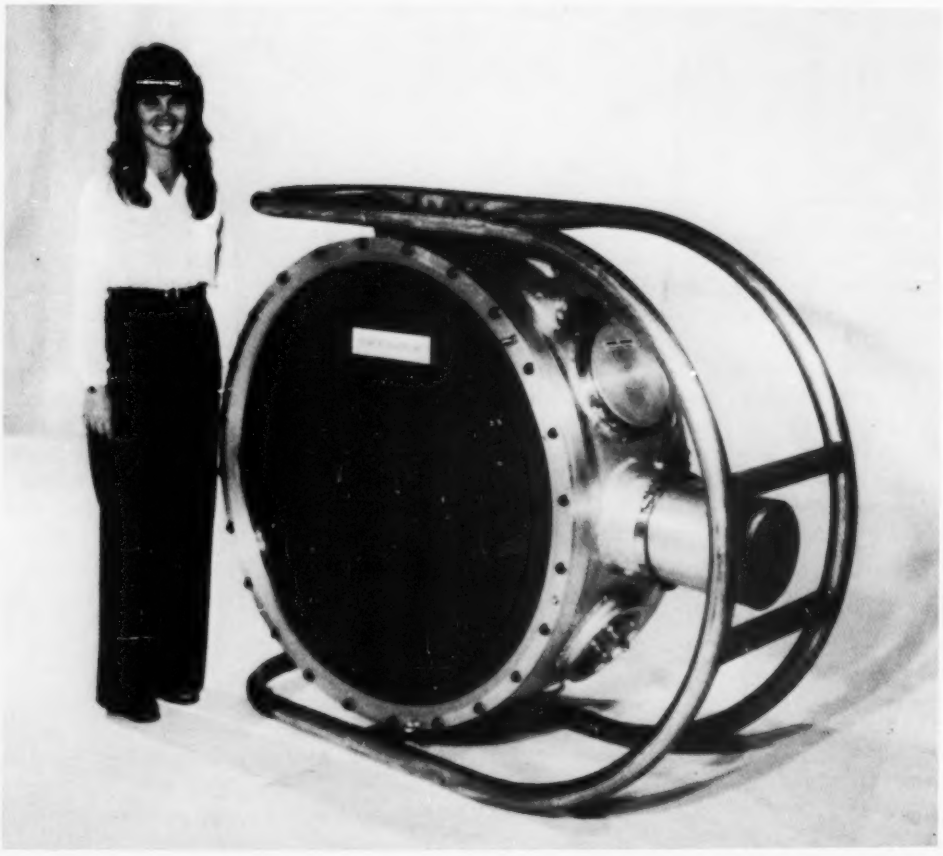

Figure 9

The source strength is peaked at about 60 Hz. Absorption and ambient noise limit the transmission to a 50 Hz to 70 Hz band.[9]

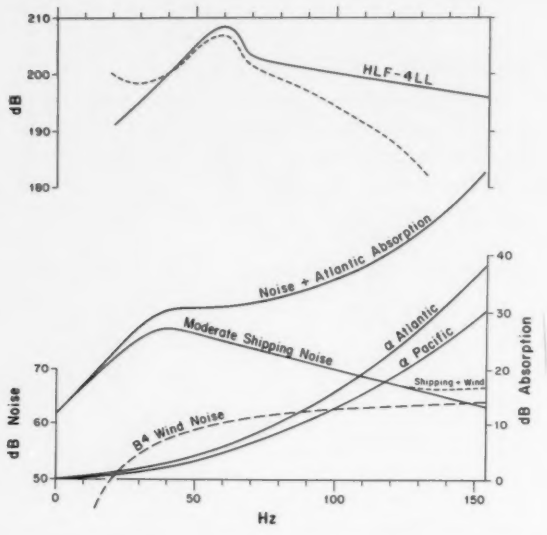

Figure 10

A ray diagram for an idealized sound channel (bottom) is associated with an arrival pattern (top) of early steep rays and late flat rays. The diagram is shown for a 700 km tomographic transmission.[10]

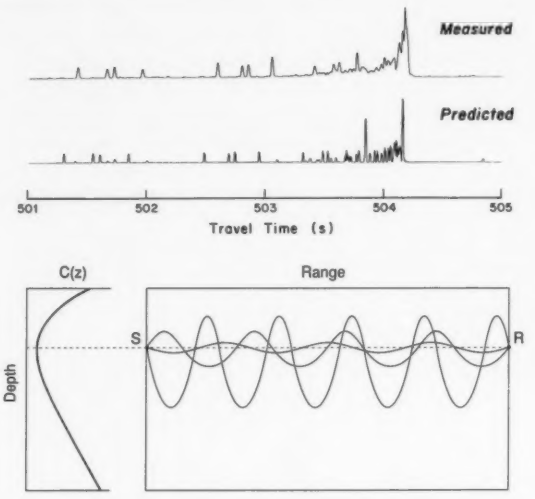

the land stations have suffered the "urban heat-center" effect. Sea surface measurements have gone from "bucket" to "injection" temperature. By coincidence, both effects require a correction of the order of 0.5°C, which is of the same order as the total change. Not a happy situation. But all these corrections have been applied with great care, and the Hansen compilation is probably as good as can be done.

The detection of the greenhouse trend is far more difficult than the detection of the CO_2 trend. The series is too short for the 4 sigma requirement. The spectrum shows a separation into low-frequency and high-frequency "noise" with a demarcation at 4 cycles per century. Gordon MacDonald separates the temperature record into three components: (1) a linear trend by 0.5°C per century, (2) high-frequency variability and (3) low-frequency variability (figure 3). Note the downward trend between 1940 and 1970.

The Hansen data suggest a 1990 rate of warming by 20m°C/year (compared to 32m°C/year for the equilibrium warming). For purposes of discussing the proposed experiment, I assume that this rate decreases exponentially with ocean depth to 4m°C/year is consistent with the observed 1960 to 1980 warming by 0.1°C below 1500m depth at the Palunirus station off Bermuda,[5] and with the 1960 to 1990 changes in the temperature of bottom water in the western Mediterranean.[6]

Going back to table 1, we note that the assumed profile in ocean warming requires a heat flux of 1.7 W/m^2 which is consistent with the incremental surface flux of 2 W/m^2 produced by the greenhouse gases. Further, that the associated rise in sea level from thermal expansion is 1.8 mm/year at mid-latitude (half this value at 60° latitude); we need to add something less than 1 mm/year from glacial melting, and end up with a rate not inconsistent with global tide gauge records. (We can use sea level as a surrogate of upper ocean heat content.) So we have a model of ocean warming which does not greatly offend a variety of evidence. To those who find fault with these numbers, I respond that the poorer the model estimates, the more important it is to replace them by observation.

How should one go about measuring global ocean warming? The simplest procedure is to install a thermometer mooring and record temperature. At 1 km depth the mesoscale eddies (the "storms" of the sea) are associated with month-to-month changes in temperature of, typically, 0.2°C rms. At the present estimated rate of warming by 4m°C/year it would take 200 years to produce a change by 4 sigma. For independent measurements from 100 moorings this estimate is reduced to 20 years. An easier way of forming an average over 100 independent samples is to take advantage of the fact that these eddies have typical dimensions of only 100 km(unlike their 1000 km atmospheric sisters) and to form a spatial line average

over distances of the order of 100 eddy scales (10,000 km). For multiple independent lines the required record length can be further diminished.

Acoustic Thermometry.

Acoustics provides a way of forming large spatial averages. The speed of sound increases by 5 m/s per °C, with a much lesser dependence on salinity. Thus the travel time between two points is a measure of the mean temperature along the acoustic path. The ocean provides a most efficient wave guide centered at the depth (normally 1 km) of the sound speed minimum (sound axis). A stick of dynamite detonated near the axis can be heard by an axial receiver clear across the Atlantic Ocean! Averaging by acoustic integration has some advantage over summing irregularly distributed land stations. There is (as yet) no problem with underwater urban heat centers. On the other hand, the depth of the sound axis varies with latitude, and we have little control over the depth dimension of the measurements.

Figure 11

A modal representation of the transmission from Heard Island to Bermuda.[11] Acoustic energy is trapped within the vertical strip between the heavy lines to both sides of the sound axis. Low modes can follow the axis without bottom interaction. High modes are "stripped" by bottom interaction.

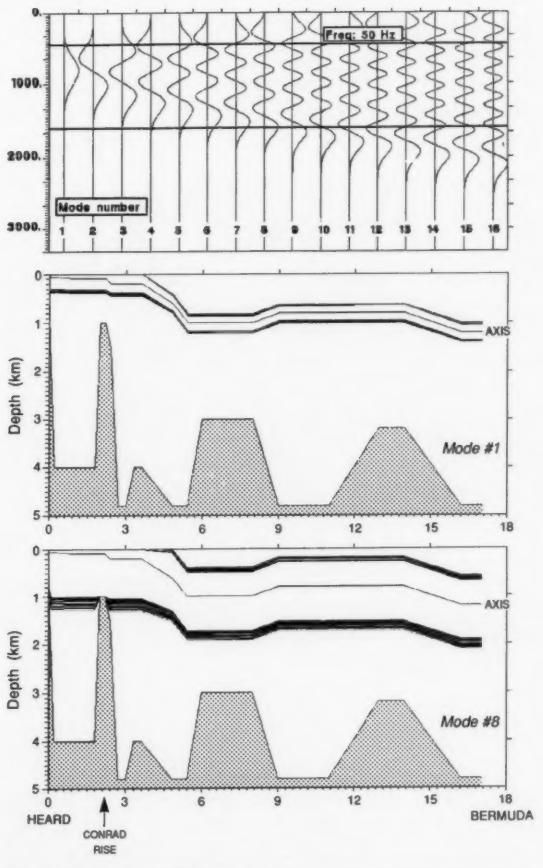

Figure 12

The vertical arrays at Monterey and Bermuda.[11] Both arrays consist of 32 elements with a 1300 m vertical aperture subtending the sound axis. The Monterey array is suspended from the surface, the Bermuda array is tethered from the bottom.

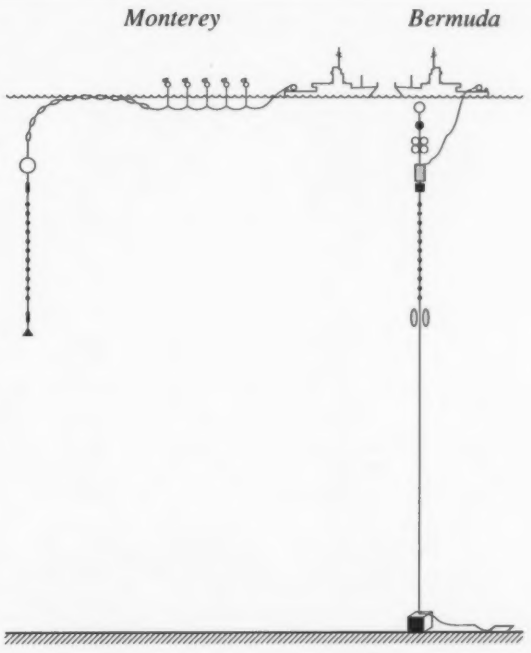

Figure 4 shows the results of an experiment conducted in 1960; a detonation off Perth was clearly detected at Bermuda half-way around the Earth![7,8] At the time the acoustic path was assumed to follow a great circle but, on an elliptical Earth, the shortest path (the geodesic) differs appreciably from the great circle. Further, one needs to allow for horizontal refraction. Using the profiles from 8000 hydrographic stations (figure 5, you can find your favorite expedition) we constructed a map of the depth of the sound axis and of the sound speed at the sound axis (figure 6). The sound axis is typically at 1 km depth,

Figure 13

Unlike ocean surface waves, sound waves are repelled by islands and seamounts.

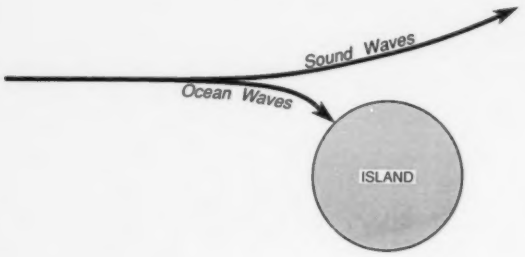

but shoals towards the high latitudes. Note the sharp gradient associated with the Antarctic Circumpolar Current, which deflects rays to the south. The previous geodesic is refracted to intersect Brazil. A clockwise rotation of the geodesic launch angle leads to an intersection with South Africa prior to reaching Bermuda. (For the moment, I assume that the acoustic energy remains trapped near the axis; the fact that the signal was detected at Bermuda is probably associated with non-axial propagation.)

Heard Island Test.

We have chosen Heard Island as an ideal site for an unimpeded transmission to Bermuda. As a bonus there is also an eastward path to San Francisco, and possibly a path through the Tasman Sea to Coos Bay, Oregon. (The curves in figure 7 are axially refracted geodesics.) We plan to transmit from Heard Island for a 10-day period beginning 26 January 1991 and to record at the 18 sites shown. This is an acoustic feasibility test, to estimate transmission and coherence losses over these paths. If successful, it is to be followed by a climate

Figure 14

It is not known whether the acoustic signal can "bounce" through the chains of islands and seamounts of Tasman Sea and the western Pacific. The bottom topography of the eastern Pacific is relatively smooth. Reproduced, by permission, from National Geographic (1969), Face and floor of the peaceful sea, pp 496-499.

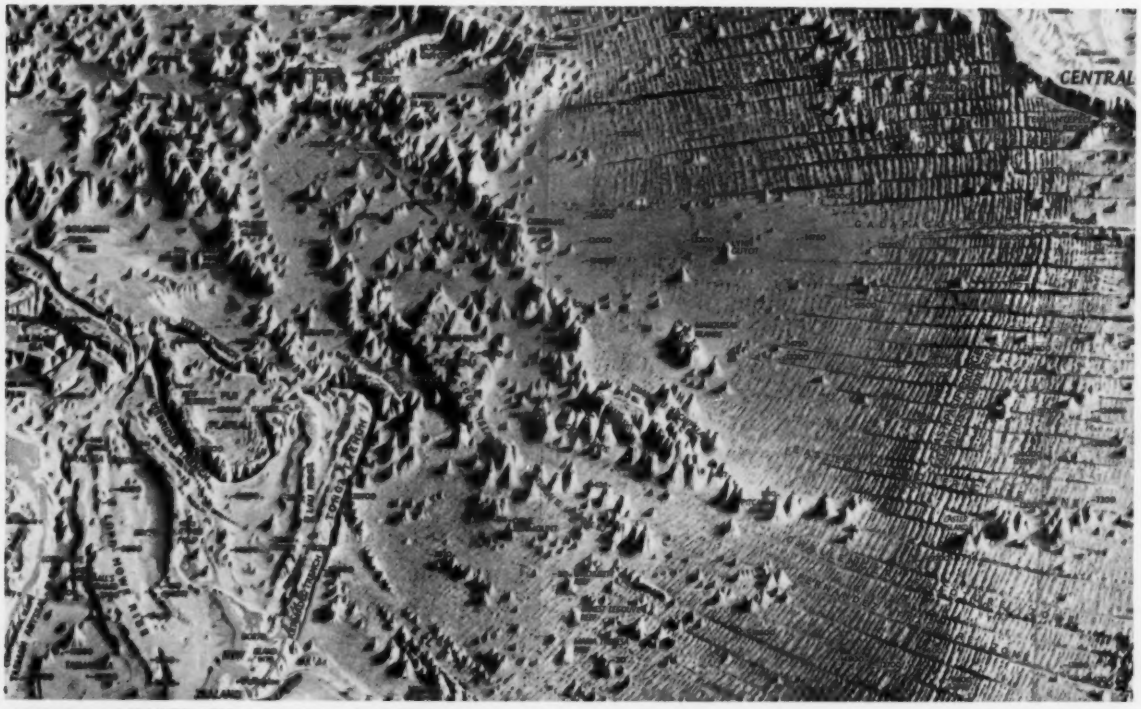

experiment extending over at least a decade using fixed sources and receivers with satellite timing.

It is not desirable to use explosive sources for obtaining time series. We will employ a source somewhat akin to a loudspeaker (figure 8). The available source is limited to depths of less than 300 m, and this requires a high-latitude location where the sound channel is relatively shallow. The source strength is 209 dB re 1 micropasqual at 1 m at the resonance frequency of 57 Hz. The source is ideally tuned for global transmissions (figure 9). At higher frequencies the attenuation becomes forbidding, and at lower frequencies the background noise (mainly shipping) is higher.

Over the past 10 years we have conducted experiments in "ocean acoustic tomography" with up to 1000 km ranges. The arrival pattern (figure 10) consists of a series of sharp pulses each identified with a given ray: steep rays arrive early; axial rays (which stay near the sound speed minimum) come in last. The predicted pattern is based on the climatological sound speed profile. The measured pattern resembles the climatological pattern, but differs in an important way. This difference permits tomographers to contour the field of sound speed (temperature) as perturbation from the mean field. (Vive la petite difference!) In the case of figure 10 the measured pattern is late and so the ocean is colder than average. It should be added that the source does not emit pulses, but rather a pseudo-random signal with a uniquely pulse-like autocovariance. The plotted arrival pattern is the correlation of the received signal with a replica of the transmitted signal.

At 1000 km ranges the pulse-like arrival pattern permits the determination of travel time with millisecond precision. At very large ranges the pulses broaden and merge, and may disappear entirely. The final cut-off is more robust. We are hoping for a precision of 10 milliseconds at 10,000 km ranges, and an intensity corresponding to at least 10 dB signal to noise ratio.

Some Unsolved Acoustic Problems.

An interpretation in terms of modes may be more fruitful (figure 11). Steep rays correspond to high modes, flat (axial) rays to low modes. Modes remain trapped along the deepening axis from Heard to Bermuda, [11] provided the change is gradual (adiabatic). The lowest mode (corresponding to the axial ray) extends about 100 m above and beneath the axis, mode 8 extends more than 500 m and intersects Conrad Rise. This results in "mode stripping" for mode numbers 8 and above. There is an interesting question whether these higher modes (steeper rays) are repopulated in 15 megameters of further travel to the most distant stations. For this purpose two vertical arrays with mode-resolving capability will be deployed off California and Bermuda (figure 12).

For glancing incidence on islands and seamounts, the sound waves are bent away from shore (opposite to surface waves, figure 13). We do not know whether the sound trans-

Figure 15

A computer simulation of travel time versus calendar time along stated paths, assuming the Princeton model of greenhouse warming (straight along sloping lines) and the Semtner model of mesoscale variability.[9]

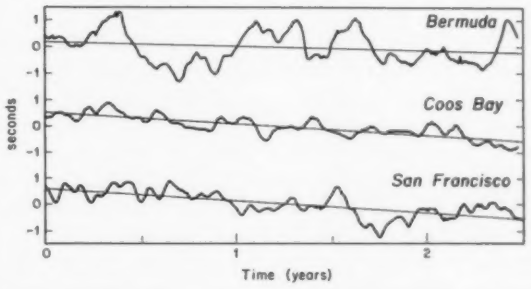

Figure 16

Wyrtky's compilation of sea level topography.[13] *In December 1975 the Pacific slopes downward to the east by about 200 mm, the opposite holds in December 1977 (an El Niño year) Sea level is a surrogate for upper ocean heat content.*

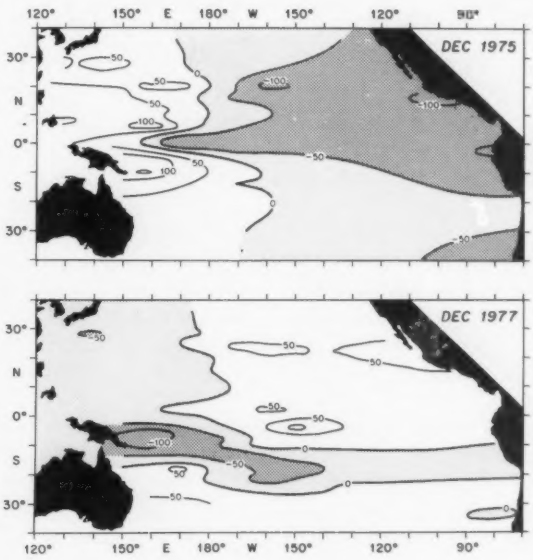

mission can bounce through the rough terrain of the Tasman Sea and the western Pacific (figure 14). The Heard Island experiment is to provide information on "global acoustics" which will determine whether a global acoustic thermometer is feasible. There are many unknowns, this is truly a feasibility experiment.

Detection of Greenhouse Trend.

The most severe problem facing a global system of acoustic monitoring is the problem of signal to geophysical (not acoustic) noise, of detecting greenhouse warming in the presence of a large natural variability. This is the same problem that has made the atmospheric determination controversial even after a century of measurements.

Using the values for ocean warming in table 1 yields a change in travel time typically by 0.25 s per year at a 15,000 km range. The straight lines in figure 15 were computed by Manabe, Spelman and Bryan (MSB) by computing the greenhouse temperature changes along the x,y,z coordinates of the three geodesics, based on their three-dimensional atmosphere-ocean model. The superposed wiggles were computed in a similar manner by Semtner and Chervin using their multilevel primitive-equation model, which exhibits mesoscale variability. The MSB model has a definite calendar time associated with the Co_2 scenario of Wuebbles *et al.*[12] The SC mesoscale wiggles are for model years 20 to 23 and have no such absolute time reference. (The SC magnitudes are strongly supported by the fact that the global distribution of the inferred mesoscale surface level oscillations is in good agreement with satellite altimetry.) For San Francisco and Coos Bay the trend is evident in only 2.5 years.

Gyre Scale Variability.

I suspect that the variability of the oceans on a larger time and space scale is a more limiting factor than mesoscale variability. Unfortunately there is very little data concerning the large scale variability. During the El Niño year in 1977 the entire northeast Pacific was higher by 100 mm than in 1975, indicating a temperature change of the upper ocean by 0.5°C (figure 16). A decadal cooling centered at Bermuda extended over most of the North Atlantic subtropical gyre (figure 17). But the North Atlantic is the only place with a sufficient database to produce maps of year-to-year changes in temperature.

In what follows we shall depend on the Hamburg ocean-atmosphere model for both the greenhouse signal and for the ambient ocean variability. Changes in sea level in 50 years following CO_2 doubling gives an indication of the spatial pattern of greenhouse ocean warming. Figure 18 shows two regions of level changes exceeding 30 cm (large and many areas with changes of less than 10 cm (small warming) or even negative values (cooling). It is totally misleading to visualize a uniform greenhouse warming. Evidently warming takes place on a gyre and ocean basin scale.

Using the same model, Uwe Mikolajewicz has computed the greenhouse induced change in soundspeed at the axis for 10 to 30 following CO_2 doubling, as well as the natural variability on 3000 model years (figure 19). The close resemblance between the mean fields of axial depth and sound speed in the model (figure 19) and from ocean observations (figure 6) lends credence to the model calculations.

For optimum detection of the greenhouse trend one would wish the fields of the greenhouse signal and of the natural variability to be orthogonal. Unfortunately this is not the case, but there are important differences between the two fields in the North Atlantic and the North Pacific. (The fact that both fields are high near Antarctica is the result of the shallow sound axis.) Figure 20 shows the probability density of 10-year trends in travel time from natural variability only (300 samples from 3000 model years) as compared to the greenhouse warming by 0.4 s/year for reception only at Coos Bay. The probability of detection is not high. However, for an imagined 36 stations at the coastal intersections of the great-circle routes, and collapsing these 36 records to two empirical orthogonal functions, the trend is well determined. From the zero'th order estimate I tentatively conclude that greenhouse warming can be detected with a suitable receiver array in something like 10 years.

Figure 17

Temperature anomaly (°C) at 1 km depth in 1975.[5]

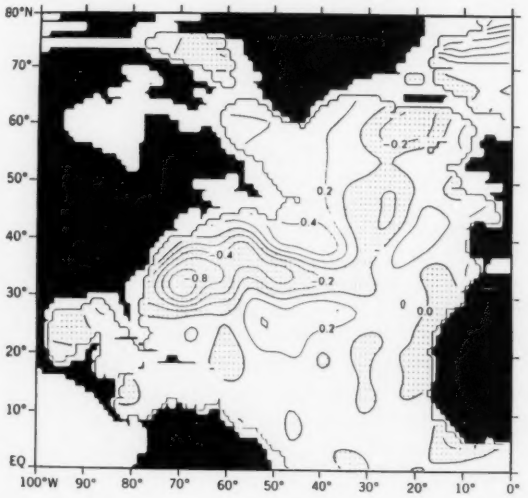

Figure 18

The change in sea level 50 years following CO_2 doubling[14]

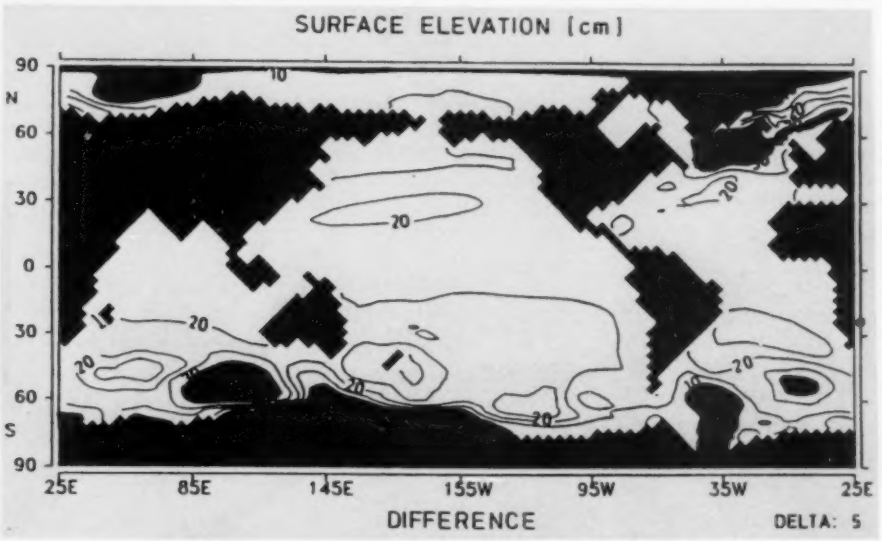

Figure 19

The left two panels give the depth and sound speed of the sound channel according to the Hamburg model.[15] *This compares favorably with the measured fields (figure 6). The right two panels show the ambient variability and the greenhouse signal, respectively, of sound speed (m/s) at the sound axis.*

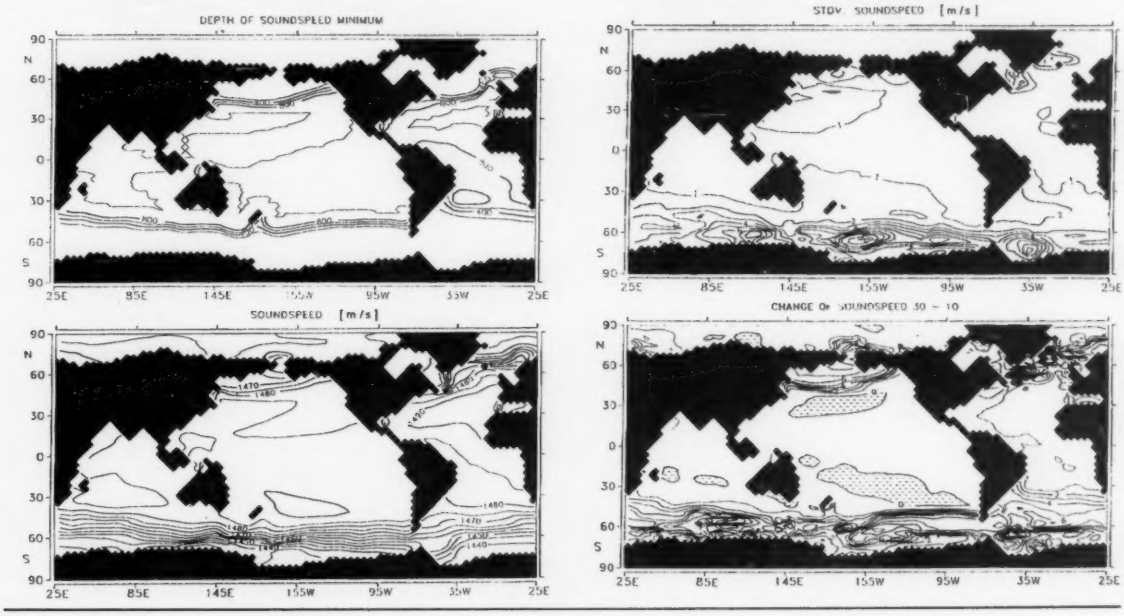

Acoustic Monitoring of Global Ocean Warming (AGLOW).

With a single source all that could be done is to validate (or invalidate) the estimates based on model calculations. For an array of sources and receivers the application of tomographic inverse theory leads to a mapping of ocean variability, including greenhouse warming. Ideally one would like an array with gyre resolution and mesoscale averaging.

Figure 21 shows the refracted geodesics from five fictitious

Figure 20

The vertical dashed line corresponds to a deterministic change in travel time by -0.4 s/year as a result of greenhouse warming. This is to be compared to the probability distribution of travel time changes (heavy line) from ambient ocean variability, based on 300 decade samples of the Hamburg model.[15] For a single path from Heard Island to Coos Bay (lower left) the signal is not significantly above the noise background, but for many paths (lower right) the greenhouse signal can be detected at about the 95% level. This result is very preliminary.

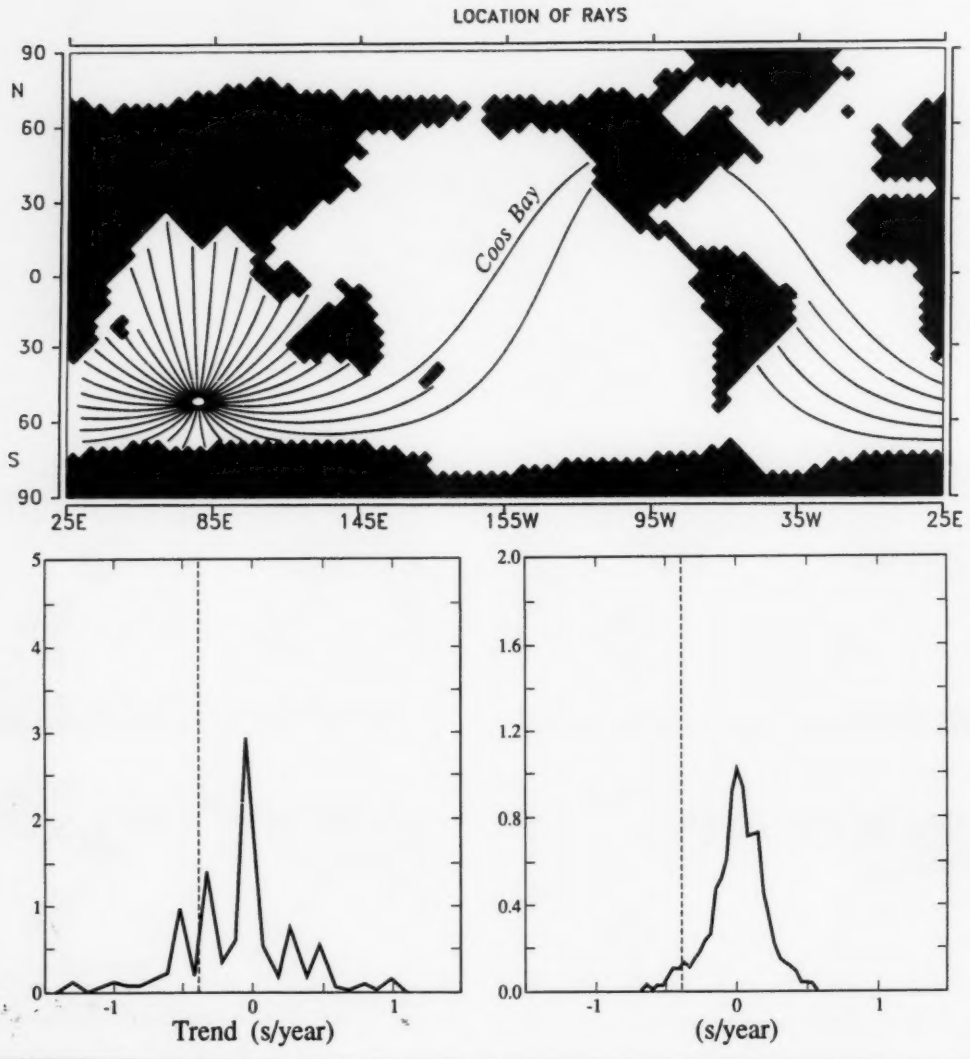

Figure 21

Axially refracted geodesics from 5 southern source locations. With such an array (purely fictitious) and 20 well placed receivers, one might begin to resolve basin temperature variability.

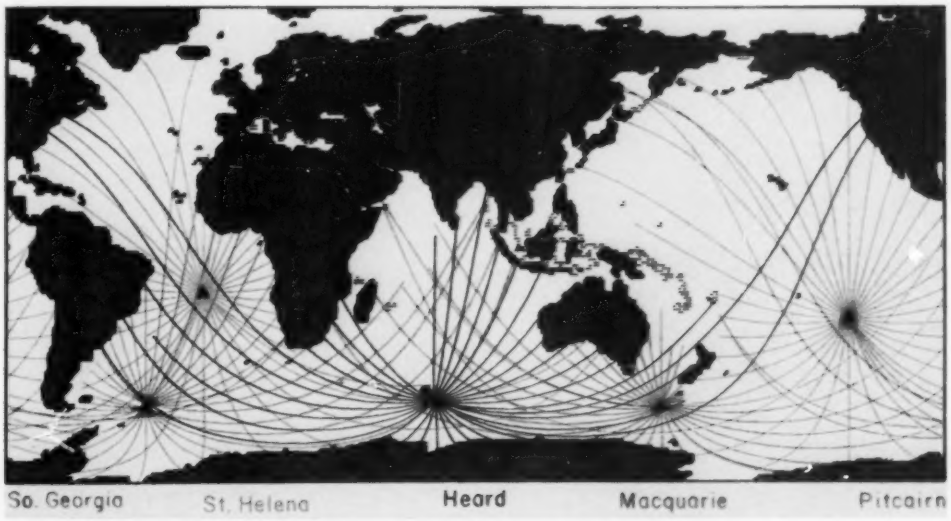

Figure 22

Some Northern Hemisphere transmissions that are under way or have been proposed. Spiesberger[16] has been studying a transmission from Hawaii to the West Coast for a number of years. There have been some transmissions from Bermuda northward across the Gulf Stream.[17] A transmission across the arctic has been proposed, and there have been Canadian-USSR discussions[18] of a Vladivostok source transmitting across the Pacific.

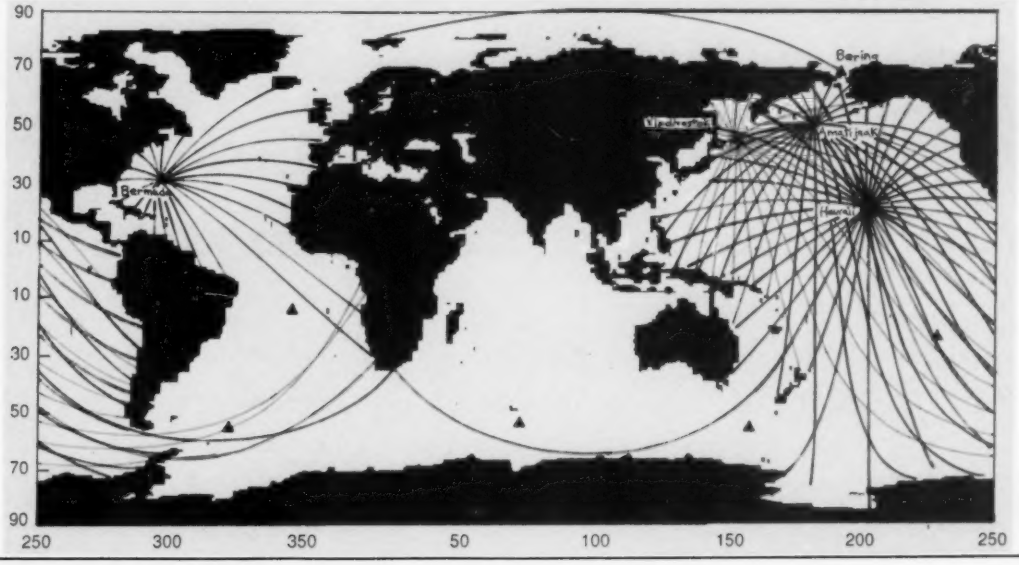

Figure 23

Source Ship Corey Chouest.

southern hemisphere sources. The distribution of oceans and continents lends itself to such a southern strategy. But there is some real activity under way (figure 22). Spiesberger has worked for five years with 4000 km transmissions from Hawaii to the American continent. Some experimental transmissions from Bermuda northward across the Gulf Stream were initiated this year. A proposal for a trans-arctic transmission is under consideration, and there have been preliminary discussions concerning a transmission from Vladivostok across the Pacific.

The central challenge is to design an affordable array of sources and receivers that optimizes the probability of detecting the greenhouse trend against the background of natural ocean variability. Most of the atmospheric work has dealt with a detection in the time domain only. An extension to the space-time domain would constitute a significant advance in our efforts to secure a timely and reliable warning.

Heard Island.

The Heard Island test is to get under way in mid-January. Robert Spindel who has built most of the equipment will be at the message center at Applied Physics Laboratory, University of Washington. Ted Birdsall and Kurt Metzger will be manning the horizontal receiver arrays off Bermuda and California. Art Baggeroer and Peter Michalevsky will be manning the vertical arrays of Monterey and Bermuda. Andrew Forbes and I will be on the source ship, and Mel Briscoe (our partner before he came to ONR) will be holding his breath back home. There are so many others whose help has been vital, Fred Saalfeld, Admiral Pittenger, John Knauss, Ned Ostenso, I cannot begin to name them.

On 9 January 1991, Andrew Forbes and I are scheduled to leave the dock at Perth. The *Corey Chouest* (figure 23) is ideally suited to the task. The sources can be lowered midship

Figure 24

Bathymetry in the vicinity of the source location surveyed by Andrew Forbes early in 1990.

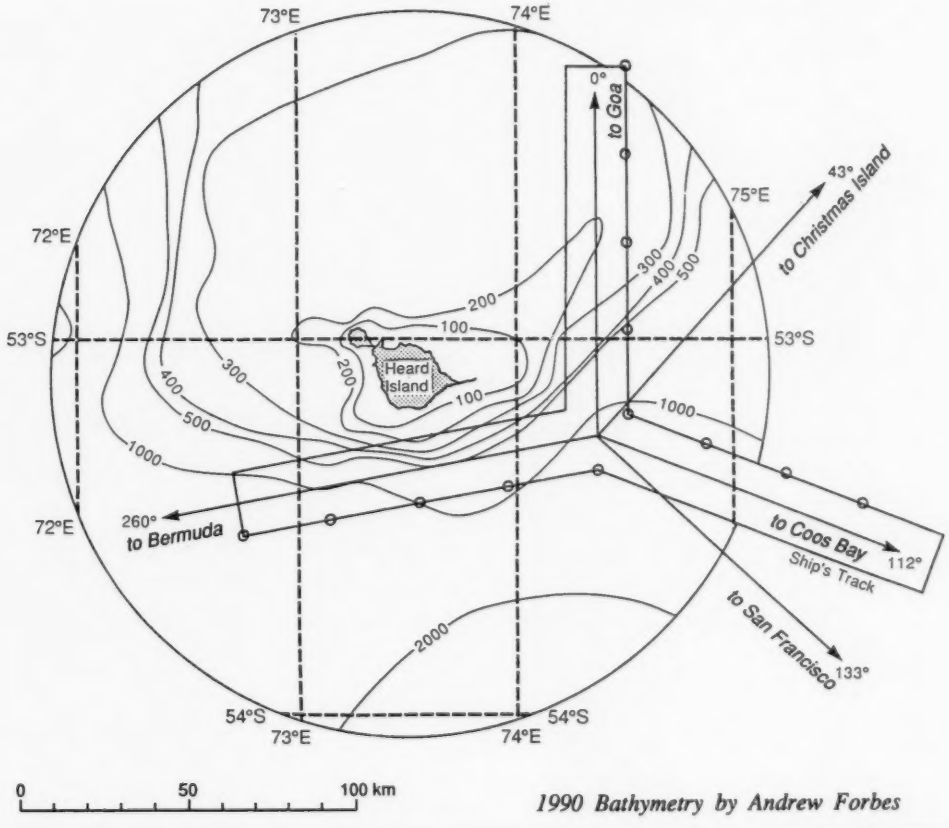

1990 Bathymetry by Andrew Forbes

Figure 25

Based on a survey by Mrs Heard in 1853. Chart of the Indian Ocean No 802 is reproduced with the permission of the Hydrographer of the Navy, United Kingdom.

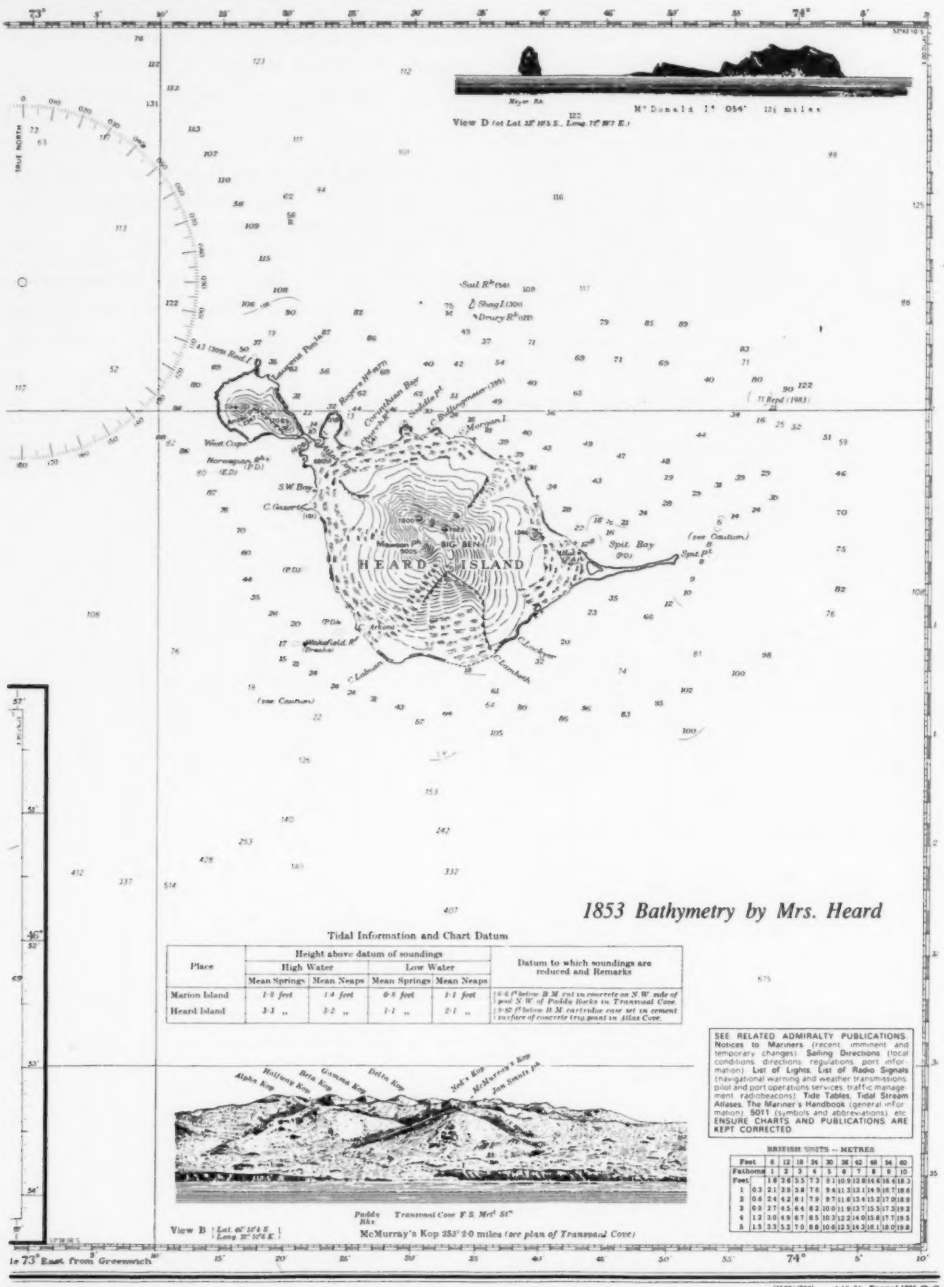
HEARD ISLAND
BIG BEN
Spit Bay
View D
View B
McMurray's Kop 253·2·0 miles
1853 Bathymetry by Mrs. Heard
Tidal Information and Chart Datum
SEE RELATED ADMIRALTY PUBLICATIONS
ENSURE CHARTS AND PUBLICATIONS ARE KEPT CORRECTED
30th June 1874, under the Superintendence of Captain F J Evans. R N C B F R S Hydrographer
80

Figure 26

Heard Island with Big Ben.

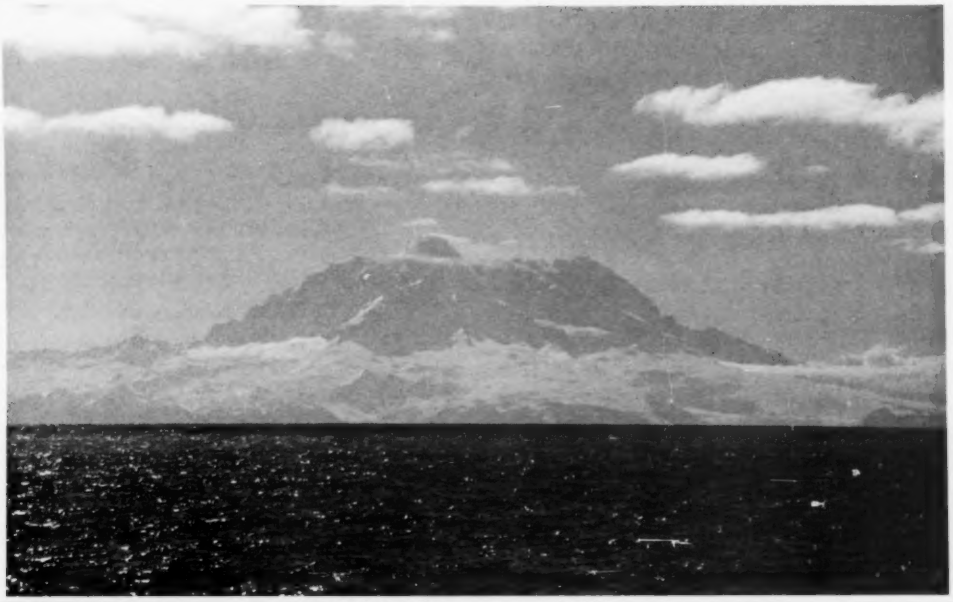

through a center well. Handling the gear over the stern could be difficult in the expected high seas. The *Corey* will be accompanied by her sister ship the *Ami Chouest* with biological observers aboard. Birdsall has worked out a 10-day schedule (one hour on, two hours off) commencing on 26 January, and consisting of 57 Hz CW(avoiding 50 Hz and 60 Hz) plus various coded sequences. Transmission time to Coos Bay is 3.5 hours. The source position 53° 15'S, 73°40'E was surveyed earlier this year by Andrew Forbes for unimpeded access to the receiving stations (figure 24). The previous survey by Mrs. Heard (Captain Heard's wife) in 1853 proved remarkably accurate (figure 25). From our position 30 nmi southeast of the island (figure 26), the 9000 ft white dome of the volcano Big Ben (climbed only once) will be towering above the clouds.

Postscript

(Excerpts from a Scripps News Release of March 15, 1991)

The first experiment to determine if sound waves can be used to measure global ocean temperatures, and ultimately, to detect the warming of the earth from a possible greenhouse effect, was successful, according to Dr. Walter H. Munk, professor of oceanography at Scripps Institution of Oceanography at the University of California, San Diego. "The question of whether an acoustic transmission can be heard globally has been answered in the affirmative," Munk said. "The quality of the transmission was good, and the reception of data is sufficient now to analyze the potential for future experiments extending over at least a decade to study global ocean warming."

Signal transmissions began January 26, 1991, and continued for four days, during which 34 transmissions were made, each lasting one hour. The sound used had about the same intensity as a foghorn. An intense storm and heavy sea conditions cut the experiment short of the 80 transmissions planned. According to Munk, nearly all of the 19 reception stations heard the signals, which took approximately three and one half hours to travel from Heard Island to the farthest station in Coos Bay, Washington.

The experiment demonstrated that the signal is of sufficient intensity to be heard, Munk said. Investigations will now focus on resolving the precision with which the codes in the signal can be used to determine arrival times and ocean temperatures. To measure the fractions of a degree of an ocean warming, it requires discerning travel times on the order of one one-hundredth of a second. Further, the experiment's results will answer the question of whether the signal could successfully travel through the mountainous seafloor topography of the southeastern Pacific Ocean. During the experiment, a team of biologists observed no significant change in the behavior of marine mammals in the vicinity of Heard Island.

References

1. Keeling, C., R. Bacastow, A. Carter, S. Piper, T. Whorf, M. Heimann, W. Mook, and H. Roeloffzen (1989). A three-dimensional model of atmospheric CO_2 transport based on observed winds: I. Observational data and preliminary analysis in *Aspects of Climate Variability in the Pacific and the Western Americans*, ed. D.H. Peterson, Geophysical Monograph **55**, AGU, Washington, D.C. 165-236.
2. Neftel, A., E. Moor, H. Oeschger, and B. Stauffer (1985). Evidence from polar ice cores for the increase in atmospheric CO_2 in the past two centuries, *Nature*, **315**, 45-47. Friedli, H. and U. Siegenthaler (1988). Influence of N_2O on isotope analysis in CO_2 and mass-spectrometric determination of N_2O in air samples, *Tellus*, **40B**, 129-133.
3. Hansen, J., and S. Lebedeff (1987). Global trends of measured surface air temperature, *J. Geophys. Res.*, **92**, 13, 345-13, 372. Hansen, J. and S. Lebedeff (1988). Global surface air temperatures: Update through 1987, *Geophys. Res. Lett.*, **15**, 323-326.
4. JASON Report JSR-89-330. The MITRE Corporation.
5. Levitus, S., 1989. Inter-pentadal variability of temperature and salinity of intermediate depths of the North Atlantic (1970-74) versus (1955-59), *J. Geophys. Res. (Oceans)*, **95**, 5233-5238.
6. Bethoux, J.P., B. Gentili, J. Raunet, and D. Tailliez, 1990. Warming trend in the western Mediterranean deep water, *Nature*, **347**, 660.
7. Shockley, R.C., J. Northrop, P.G. Hansen, and C. Hartdegen, 1982. SOFAR propagation paths from Australia to Bermuda: Comparison of signal speed algorithms and experiments, *J. Acoust. Soc. Amer.*, **71:1**, 51-60.
8. Munk, W.H., W.C. O'Reilly, and J.L. Reid, 1988. Australia-Bermuda sound transmission experiment (1960) revisited, *J. Phys. Oceanogr.*, **18**, 1876-1898.
9. Munk, W.H., and A.M.G. Forbes, 1989. Global ocean warming: An acoustic measure? *J. Phys, Oceanogr.*, **19**, 1765-1778.
10 Worcester, P.F., B. Dushaw, and B. Howe, 1990. Gyre-scale reciprocal acoustic transmission. Presented at SACLANT Undersea Research Centre Workshop on Ocean Variability & Acoustic Propagation, 4-8 June, 1990, La Spezia, Italy.
11. This figure was supplied by A.B. Baggeroer (personal communication) who is responsible for the design of the vertical arrays in Figure 12.
12 Wuebbles, D.J., M.C. MacCracken, and F.M. Luther, 1984. A proposed reference set of scenarios for radiatively active constituents. United States Department of Energy, Washington, D.C. (DOE/NBB-0066). [Available from NTIS, Springfield, Virginia.]
13. Wyrtki, K., and S. Nakahoro (1984). Monthly Maps of Sea Level Anomalies in the Pacific 1975-81. Hawaii Institute of Geophysics Report HIG-84-3.
14. Mikolajewicz, U., B. Santer, E. Maier-Reimer (1990). Ocean response to greenhouse warming, *Nature*, **345**, 589-593.
15. I am greatly indebted to U. Mikolajewicz and E. Maier-Reimer for analyses of acoustic travel times based on the "Hamburg Model" (See Hasselmann, K., 1982, An ocean model for climate variability studies, *Progr. Oceanogr.*, **11**, 69-92.
16. Spiesberger, J.L., 1990. Basin-scale tomography: Synoptic measurements of a 4000-km length section in the Pacific. *J. Phys. Oceanogr.*, **19**, 1073-1090.
17. Howe, B.M., J.A. Mercer, R.C. Spindel, T.G. Birdsall, K. Metzger, Jr., P.F. Worcester, and B. D. Cornuelle, 1990. Applied tomography: Monitoring the Gulf Stream, *EOS*, **71**, 1409.
18. Farmer, D., 1990, personal communication.

Biography

Professor Munk received his bachelor of science and master of science degrees from the California Institute of Technology in 1939 and 1940 respectively, and his doctorate in oceanography from the University of California in 1947. He has spent the greater part of his professional career at the University of California in San Diego, and the Scripps Institution of Oceanography. He rose from assistant professor to full professor in the period 1947-1954. In addition to Professor of Geophysics, Professor Munk has served as Associate Director of the Institute of Geophysics.

Today, Professor Munk holds the Secretary of the Navy Research Chair in Oceanography at the Scripps Institution of Oceanography, University of California, San Diego. In 1985 he received the National Medal of Science from President Reagan. He is a member of the National Academy of Sciences, the American Philosophical Society, and the Royal Society of London. He holds honorary degrees from the University of Bergen and Cambridge University. Last year he received the Bowie Medal of the American Geophysical Union.

Profiles in Science

Calvin F. Quate

Professor Calvin F. Quate, who is Chairman of the Department of Applied Physics, has been at Stanford University since 1961. Among his contributions to science under Office of Naval Research funding, he was responsible for the realization of the "ultimate" scanning acoustic microscope, a cryogenic instrument with submicron spatial resolution. He received much recognition for this work, including the IEEE Medal of Honor in 1988. Professor Quate is a member of several professional societies and a fellow of the National Academy of Sciences and the National Academy of Engineering.

With his background in scanning microscopies, Quate was quick to recognize the vast potential of the scanning tunneling microscope (STM), both as a scientific tool and as a means to develop new technologies featuring sizes in the nanometer range. With colleagues at Stanford, he produced a new technique known as atomic force microscopy (AFM). Similar to STM, AFM can image individual atoms on the surface of a solid, but does not require that the surface be electrically conducting. Using these two techniques of STM and AFM, Quate and his coworkers have undertaken a series of pioneering studies.

They have explained the patterns formed by adsorbate atoms on various semiconductor surfaces. They have imaged individual polymer strands and have shown how these strands can be manipulated by voltage pulses. Also they have been responsible for substantial progress on the technological side, in particular, by developing microfabrication techniques for batch fabricating AFM cantilevers and tips. Professor Quate's current interests include tunneling acoustic microscopy and the storage of digital information.

Results of an Efficient Gating Algorithm for Large-Scale Tracking Scenarios

Jeffrey K. Uhlmann and Miguel R. Zuniga
Naval Research Laboratory

Abstract

The correlation of sensor reports with targets, or clusters of targets, represents a significant combinatorial bottleneck for multiple-target tracking systems designed for large-scale scenarios. A variety of practical considerations are discussed in the context of the TRC tracking and correlation system developed at the Naval Research Laboratory for use in the SDI National Testbed. Test results of one approach to the problem are presented for scenarios involving over one million targets. Parallelization approaches are discussed which suggest that it is feasible to process such scenarios in real-time on presently available parallel and multiprocessing architectures.

Introduction

Gating is an important component of most multiple-target tracking systems. Its function is to identify sensor reports, e.g., radar or IR returns from missiles, planes, etc., which correlate highly with current state estimates (i.e., tracks). For small numbers of objects, it is feasible to calculate a probability of correlation for every track/report pair and reject those whose measures of correlation fall below some threshold. For large numbers of objects, however, the quadratic growth in the number of pairs for which correlation probabilities are computed by this "brute force" approach represents an enormous bottleneck. This combinatorial problem is of particular concern in SDI tracking and correlation for which numbers of objects on the order of 10^5-10^6 must be processed in *real time*. It is also of great concern to air defense systems for short-range assaults in which trajectories of 10-100 targets must be determined within minutes of detection.

The TRC is a multihypothesis tracker/correlator developed at the Naval Research Laboratory for conducting experiments in multiple-target tracking. Early tests of the TRC revealed that combinatorial problems severely limited the size of the scenarios that could be examined. Subsequent analysis demonstrated that these limitations were the result of a correlation (gating) algorithm which scaled quadratically in the size of the scenario. Research into approaches for reducing this computational complexity identified two primary difficulties: (1) The correlation threshold, or gating criterion, depends upon error covariances that are generally unique to each track and report. (2) The measurement times of the reports are generally distributed over some non-zero time interval, yet the correlation measurement function is defined only for track/report pairs that are valid at the same time. These two factors appear to demand the comparison of every track to every report. However, it has been shown in [1], [2], and [3] that multidimensional tree data structures can be used to perform efficient

gating without sacrificing accuracy of the overall tracking process. In this paper the authors discuss the practical application of these data structures to the TRC and present results of tests performed on scenarios consisting of more than one million objects. Parallelization considerations are also discussed.

Gating in the TRC

The gating problem can be stated technically as follows: Given a motion model and a set of tracks consisting of current state estimates with associated error covariances and a set of sensor reports consisting of measurement timestamps and position measurements with associated error covariances, determine in real time which pairs (i,j) satisfy the gating criterion:

$$S_{ij}(dX_{ij}^t, \Gamma_{ij}) = \frac{\exp(-dX_{ij}^t \Gamma_{ij}^{-1} dX_{ij}/2)}{(2\pi)^{\frac{d}{2}} \sqrt{|\Gamma_{ij}|}} \tag{1}$$

and

$$S_{ij} \leq S_i, \tag{2}$$

where d is the measurement dimension, dX_{ij} is the residual vector difference of report i and track j (projected to the time of the report), Γ_{ij} is the residual covariance of the pair, and S_i is the gating threshold selected as per report. The efficient identification of pairs that satisfy the gate can be accomplished by deriving from the gating threshold a search volume for each report, thus limiting the number of correlation candidates which must be examined. This transforms the problem from probability space into Euclidean space where efficient computational geometric methods can be applied. The calculation of the volume depends upon the report and track covariances, the gating threshold, and the maximal time differentials between the current states of the tracks and the observation times of the reports. Methods for calculating this search volume are developed in [1] and [2]. In many systems, however, this step is partially obviated by the necessary maintenance of assumed causally independent (in terms of the above correlation measure) clusters of tracks. Thus, gating becomes a problem of associating reports with clusters.

TRC Clustering

Spatial clusters are maintained by TRC in order to reduce the multiplicity of hypotheses (tentative track/report pairings) generated by its multihypothesis tracking (MHT) algorithm. The clusters are defined by a minimum separation criterion which requires that an object be a member of a given cluster if and only if it is within the minimum separation distance (MSD) of another member of the cluster. This minimum separation distance is determined by the correlation measure, the motion characteristics of the targets, and the resolution of the sensor(s) and is intended to impose a causal partition of the object set. Since the MHT algorithm requires a correlation measure to be computed for every track/report pair associated with a particular cluster, the role of the gating algorithm is to assign incoming reports to their appropriate track clusters. If there are N_R reports and N_C clusters, a brute force approach would scale as $N_R N_C$ and thus would be appropriate only for

Figure 1

CPU times of the search algorithm fitted with an NlogN function (solid line). N = the number of tracks = the number of reports. T is the search time in seconds. Simulation performed on a Sun4 workstation.

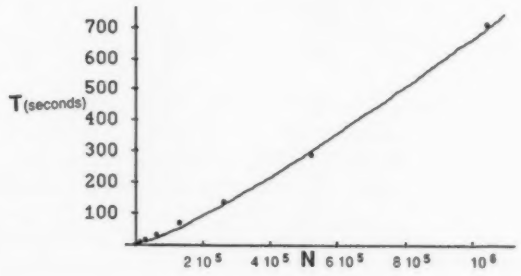

small N_C. However, because N_C is purely data dependent and in general approaches N_R as the tracking process converges, a more sophisticated approach is necessary to reduce the upper bound computational complexity.

In the TRC model, track clusters are represented by what are termed pseudotracks. A pseudotrack is a track structure constructed by averaging over tracks within a cluster. Specifically, its position is the mean of the cluster and its covariance is computed so as to approximate the covariance distribution of the tracks within the cluster. The Gaussian density with mean μ and error covariance Σ for a cluster C is defined [4] as:

$$\mu = \sum_{j=1}^{N} w_j \mu_j \tag{3}$$

$$\Sigma = \sum_{j=1}^{N} w_j \Sigma_j + (\mu_j - \mu)^T (\mu_j - \mu), \tag{4}$$

where each w_j represents a weighting factor reflecting the likelihood of association of the jth track/report pair based upon the feasible track/report matchings in which it appears. Since the dynamics of objects within the same cluster are assumed strongly correlated, pseudotracks permit the treatment of clusters as if they were single track objects. Use of these pseudotracks can achieve the brute force $O(N_R N_C)$ scaling mentioned above. In order to improve upon this scaling, a method is required that avoids the projection of every pseudotrack to the time of every report. This can be accomplished by utilizing the already assumed MSD threshold. For example, a search radius can be computed for each cluster by projecting the tracks through the scan period and determining the maximum distance any track (or more precisely, any point within any member track's thresholded covariance volume) reaches from the centroid of the cluster and adding the MSD. This defines a search volume for each cluster within which every correlated target should be found. Since the search volumes are not in general disjoint, it is necessary to apply a secondary test in order to resolve ambiguous cases. In the TRC this is accomplished by computing a correlation score for each such report with the pseudotracks of the clusters with which it gates.

To treat correlation as a point enclosure problem requires that either the tracks or the reports be point objects. However, both sets consist of volumetric objects since each report is generally associated with a thresholded covariance volume. A simplistic solution to this problem is to *deflate* one of the sets by adding the maximum radius of its elements to the radius of each element of the other set. In cases where the distribution in radii of the elements of the two sets is broad, this approach may introduce a large degree of inefficiency and the more sophisticated strategy described in [2] may be required.

Efficient Searching

In order to efficiently identify the tracks within the gating radius of each report, the tracks must be placed into a search structure from which the desired set can be retrieved without having to examine every track. (Actually, if the number of reports greatly exceeds the number of tracks, it may be more efficient to construct the search structure from the set of reports. This consideration is discussed more fully in the next section.) Data structures with storage requirements proportional to the number of tracks, N_T, are known which provide this capability [4]. They require only $O(N_T \log N_T)$ setup time and between $O(d \log N_T + k)$ and $O(N_T^{1-\frac{1}{d}} + k)$ average retrieval time, where k is the average number of tracks found per report and d is the number of dimensions of the search space. However, our investigations have revealed that a variation of one of these data structures provides a small linear improvement in the average retrieval time when the computed radius is small relative to the average inter-object separation [7]. Techniques for exploiting distribution features of targets have also been used to significantly reduce retrieval time [8].

The degree to which efficient search algorithms can be applied depends heavily upon the difference in dimensionality between the state estimates, or tracks, and the sensor measurements, or reports. Often tracks will maintain estimates of position and one or more of its derivatives (and possibly some number of target attributes such as temperature or size). If one or more of these parameters must be derived from multiple reports, the reports are said to be *subdimensional*. For example, bearing-only measurements from IR sensors are subdimensional with respect to position. When measurements are of full positional dimensionality, correlation of tracks and reports requires satisfaction of what are known as *orthogonal range queries*. Satisfaction of a range query determines the elements of a point set which fall within an isothetic, i.e., coordinate-aligned, hyper-rectangle defined by ranges in each of the measurement dimensions. If the measurement dimensions are not orthogonal, an appropriate coordinate transformation or projection is required. If the measurements are subdimensional, however, no such transformation may exist and the use of efficient search algorithms may be precluded.

Since the TRC system is designed to process IR as well as radar reports, the issue of subdimensional correlation becomes important. Specifically, the correlation of tracks and bearing-only reports defines a class of query volumes which in principle are of infinite extent along the sensor line of sight. A simple limitation on the maximum distance any target can be assumed from the sensor results in finite search volumes; unfortunately, the approximation of such regions by isothetic volumes may be inadequate for efficient search. Another option is to transform the tracks to the spherical coordinate system of the sensor and define 2-dimensional range queries in the measurement angles. This approach is very efficient in the case

of one sensor. In the case of multiple sensors, however, the transformation steps scale as the product of the number of tracks and the number of sensors. If the ratio of sensors to tracks is small, this may not be an important consideration. If not, a different approach is required. In the case of satellite-based IR sensors, however, knowledge that the line of sight vectors tend to be tangent to the earth can be exploited to good advantage. Specifically, the transformation of all tracks to an earth-centered spherical coordinate system allows the sensor measurement regions to be relatively well approximated by ranges in the two angular coordinates. The scaling of this approach is then relatively independent of the number of sensors.

The Multiple Timestamp Problem

The fact that the computation of the gating radius must take into account the maximal time differential between the report measurements and the latest track updates leads to a source of possible inefficiency. In particular, the search volumes scale approximately as the cube (in three dimensions) of the time differential. Thus, if the report measurements are made over a very long scan period, the gating radius may become impractically large. In order to alleviate this problem, a technique has been devised by which copies of the complete set of tracks are projected to time intervals throughout the scan period. This ensures that the maximum time differential used for any report is no more than the length of the scan period divided by twice the number of projections. Furthermore, a function has been derived that computes the number of projections required to optimize the tradeoff between the computational cost incurred by a large time differential and the cost of making multiple track projections. A thorough complexity analysis (see ref. 1) reveals that this geometric dilution strategy permits better than quadratic scaling even for scenarios involving very long scan periods.

An important consideration when minimizing the average track/report time differential by subdividing the scan period is whether to perform the searching operations required for correlation on the track or report datasets. Searching on the track dataset results in the following scaling for the overall gating process for reasonable †target density and scan length:

$$\text{Setup time} = O(mN_T \log N_T)$$

$$\text{Search time} = O(N_R(\log N_T + k)), \tag{5}$$

where m is the number of subdivisions of the scan period and k is the average number of objects found per report. This scaling corresponds to the construction of m search structures and the performing of N_R searches on those structures. The resultant scaling for searches on the report dataset for similar scenarios is approximately:

$$\text{Setup time} = O(m(N_R/m)\log(N_R/m))$$

$$\text{Search time} = O(mN_T(\log(N_R/m)+k)), \tag{6}$$

where the values m and k are not in general the same as in former case. This case corresponds to a binning of the reports into m bins of N_R/m reports according to their timestamps and constructing a search structure for each bin. (This binning process for unordered reports can be performed in worst-case linear time using a simple variation of standard median-finding algorithms.) The scaling of the search process corresponds to a projection of each track to the middle of the time interval associated with each of the m bins and performing a search.

A cursory examination of the relative scaling behavior of the two approaches reveals that the former should provide better performance when N_T greatly exceeds N_R while the latter may be preferred when N_R greatly exceeds N_T. Thus, the former approach might be preferred in an MHT system (that does not employ clustering) in which the number of hypotheses is expected to be many times greater than the number of reports. For example, scenarios involving small numbers of short-range missiles may require the generation of thousands of hypotheses to assure that trajectories are determined early enough for assignment and deployment of antimissile missiles.* The latter approach would be preferred when tracking is performed in heavily cluttered environments where the number of tracked objects is much less than the number of reports. In cases where N_T and N_R are expected to be roughly comparable, the former approach may be preferred because it avoids the m factor in the computationally more expensive search step.

In MHT systems such as the TRC where the assignment algorithm requires a correlation measurement for every track/report pair associated with the same cluster, only the pseudotracks must be considered by the gating algorithm. As far as the gating algorithm is concerned, then, $N_T = N_C$. When N_C is much smaller than N_R, the construction of search structures from the report datasets is probably more appropriate. In the case of the TRC, however, the choice was made to construct search structures from the track datasets because (1) N_C should approach N_R as the tracking process converges, and (2) communications constraints in some proposed SDI battle management environments effectively require that reports be processed as they

† The term reasonable in this context can be rigorously defined using results presented in ref. 1. These results assume that the search step can be performed in average-case O ($N \log N$) time.

* Current antimissile defense systems, such as the Patriot, require independent targeting and assignments and thus are severely limited in their effectiveness against clusters of targets.

are received, thus precluding the batch processing required to construct search structures from reports.

Test Results

In order to verify the predicted run-time behavior, the authors tested the critical search component of the algorithm on single timesteps (or scan periods) from scenarios ranging in size from $N_R = N_T = 1024$ ($1K$) to over one million ($1M$) objects. Target density was maintained so that for each scenario ~ 5 reports gated with each track. Results in Figure (1) suggest that for the numbers of objects tested, the scaling of the search algorithm is dominated by $O(N \log N)$, though careful analysis suggests the possibility of small contributions from higher order (e.g., $N\log^2 N$) terms. It should be emphasized that the results do not include the time spent evaluating Equation (1) since the interest here is in scaling behavior; however, it should be noted that for a ten second scan period as many as $16K$ gates can be identified in *real-time*. It is also interesting to observe that only a factor of 75 speedup over the Sun-4 used in our tests is required to process one million objects in real-time. Such a speedup seems quite feasible on several currently available multiprocessing or parallel computers.

Parallel Processing Considerations

The techniques described above for correlating sensor reports with target clusters can also be employed for correlating reports with *clusters of clusters*. This provides a mechanism for partitioning the tracking problem for parallel execution. Specifically, a spatial partition of the tracking environment into P regions, where each region has approximately the same number of targets, enables targets within each region to be assigned to one of P processors in $\log P$ time. (The trajectories of the elements of these super clusters can be assumed correlated in SDI scenarios since their destinations are assumed to be correlated. Thus, a pseudotrack representation like that described above can be used.) This decomposes the total gating problem into P independent gating problems of size N/P, $N \approx N_R \approx N_T$, which can be processed in parallel. The overall scaling, then, is $O((N/P)\log(N/P) + \log P)$.*

A second approach to parallelization is particularly efficient for scenarios in which the ratio of targets to reports is extremely small (e.g., N_R is much larger than N_T due to clutter). In this approach a search structure is constructed from the set of tracks on each of the P processors. The reports can then be assigned in any balanced fashion for processing on any of the processors. This technique scales as $O((N_R/P)\log N_T)$ and, like the previously described approach, requires virtually no interprocessor communication. Thus, an $O(P)$ speedup should be expected on a P-processor MIMD machine. Multidimensional tree structures can be mapped efficiently onto SIMD architectures, such as the Connection Machine, to achieve similar scaling [9]. NRL has both MIMD and SIMD architectures (BBN TC-2000 and Connection Machine, respectively) on which the authors are presently examining additional parallel implementation issues.

Discussion

A module developed from this study of the gating problem has been incorporated into a version of the TRC tracking and correlation system used in the SDI National Testbed. Results of tests on SDI-type scenarios reveal that the new gating approach scales approximately as $N_R \log N_C$ and provides significant performance improvements over brute force even for small numbers (40-50) of objects in the small scan length case. Additional tests of a stand-alone module demonstrate that the multiple projection strategy can maintain this scaling for scan lengths of 10 seconds or more. Even for scan lengths an order of magnitude larger, however, subquadratic scaling can be expected. Serial implementations of the module permit simulations to be run using scenarios consisting of more than one million objects. Incorporation of some of the techniques described in this paper into a tracking system installed on a Sun workstation has permitted 65-100 targets to be tracked in real time — including initial detection and track initiation[10]. Parallel implementations are expected to provide even more dramatic results.

Biographies

Jeffrey K. Uhlmann and Miguel R. Zuniga have conducted basic research in the area of tracking and correlation for over 4 years at the Naval Research Laboratory in Washington, DC. Their emphasis has been toward the application of sophisticated data structures and recent results from the field of computational geometry to reduce the combinatorics of multiple-target tracking. Together with colleagues J. M. Picone and J. B. Collins, the authors have been awarded NRL recommendations for two patent applications related to multiple-target correlation.

* A more sophisticated mapping of the tree structure onto the processors can eliminate the need for cluster assignments and reduce the $N \log P$ term to $(N/P) \log P$.

References

1. M. R. Zuniga, J. M. Picone, and J. K. Uhlmann, "Efficient Algorithm for Improved Gating Combinatorics in Multiple-Target Tracking, submitted to *IEEE Transactions on Aerospace and Electronic Systems*, (4/90).
2. J. B. Collins and J. K. Uhlmann, "Efficient Gating in Data Association for Multivariate Gaussian Distributions," submitted to *IEEE Transactions on Aerospace and Electronic Systems*, (2/90).
3. J. K. Uhlmann, M. R. Zuniga, and J. Michael Picone, "Efficient Approaches for Report/Cluster Correlation in Multiple-Target Tracking Systems," NRL Report 9281 (1990).
4. "SDI Tracker/Correlator Design Document (third ed.)," report from Ball Systems Engineering Division and Daniel H. Wagner Associates delivered to NRL, (4/89).
5. Kurt Mehlhorn: Multidimensional Searching and Computational Geometry, EATCS monograph, Springer-Verlag Berlin (1984).
6. Hanan Samet: The Design and Analysis of Spatial Data Structures, Addison-Wesley Publishing Co., New York (1990).
7. Jeffrey K. Uhlmann, "Enhancing Multidimensional Tree Structures Using a Bi-Linear Decomposition," NRL Report 9282, (1990).
8. Jeffrey K. Uhlmann, "Adaptive Partitioning Strategies for Ternary Trees, submitted to *Pattern Recognition Letters*, (11/90).
9. Guy E. Blelloch: *Scan Primitives and Parallel Vector Models*, Ph.D, dissertation, Dept. of Electrical Engineering and Computer Science, Massachusetts Institute of Technology, (1988).
10. J.B. Collins and J.K. Uhlmann, "REAL Approach to Tracking and Correlation for Large-Scale Scenarios," *NRL Review* (1989-1990).

Development of a Planar Fiber Optic Hydrophone for Measuring the Low Wavenumber Pressure Components of Turbulent Boundary Layers

P.C. Shang, P.J. Zoccola, S.A. Fisher, Y.F. Hwang
David Taylor Research Center

The Office of the Chief of Naval Research sponsors the Independent Research (IR) and the Independent Exploratory Development (IED) Programs at 11 R&D centers including the David Taylor Research Center (DTRC), Bethesda, Maryland. Over the years, DTRC's programs have produced and fostered many innovative concepts in naval design including the development of: high-strength low-alloy steels that reduce ship costs; stealth concepts to decrease the vulnerability of both submarines and ASW surface ships (skewed propellers and acoustic coatings for LOS ANGELES and SEAWOLF submarines); real-time data fusion methods; low drag ship hull shapes; advanced armor concepts; and improvements in composite materials.

In the 1990's, new technologies will revolutionize the design of future Navy ships. The IR/IED programs will enable the Navy to support critical technologies such as the development of: microelectronic circuits, machine intelligence, signal processing, signature control, pulsed power, advanced materials, and superconductivity.

The IR/IED programs in the last year produced 22 refereed journal articles, six patent disclosures, 44 major presentations to scientific societies, 29 reports, one book and one dissertation. From these noteworthy contributions to the scientific literature, the following article documents a technical accomplishment which was judged to be the best FY-89, IED project on the basis of technical merit, potential impact on Navy/Center needs and productivity.

(Editor's Note)

Abstract

This paper discusses the developments of a planar fiber optic hydrophone, particularly its application to measuring low wavenumber contents of fluctuating pressures underneath a turbulent boundary layer. These wall pressure fluctuations, when characterized by the wavenumber-frequency spectrum, have most of the fluctuating energy lying in the convective domain. In the coupling between large structures and low speed fluid flow, however, the subconvective, or low-wavenumber, domain becomes the dominant contributor. Although the low wavenumber domain has been an area of active experimental and analytical investigations for more than two decades, researchers have not attained a validated description of the low wavenumber domain. Studies of the coupling between structure and flow have mainly relied on semi-empirical models of the wavenumber-frequency spectrum. Contaminations by the convective and acoustic domains are two factors affecting the ability to obtain accurate low wavenumber measurements. A large fiber optic hydrophone has been developed by taking advantage of the inherent geometric flexibility of fiber optic hydrophones. The reduction of the convective contribution through area averaging produces a fiber optic hydrophone with low flow noise. Unique features of the hydrophone include its insensitivity to vibrational noises and acoustical transparency. The hydrophone design was initially selected for the Low Cost (Fiber Optic) Planar Arrays (LCPA) Advanced Technology Demonstration (ATD).

Figure 1:

Schematic of the planar fiber optic hydrophone system.

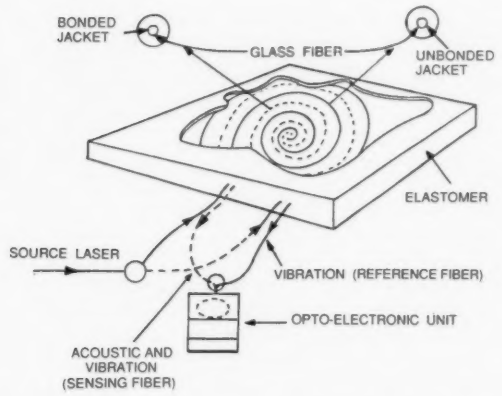

The planar fiber optic hydrophone may provide additional information about the flow induced noises of hydrophones and hydrophone arrays. Calculations were made to demonstrate the potential of the planar fiber optic hydrophone for quantifying the low-wavenumber domain. Finite element models have also been developed for predicting the acoustic sensitivity of fiber optic hydrophones. Finite element analysis successfully predicted the measured sensitivity of the planar fiber optic hydrophone.

Introduction

Fiber optic sensors are capable of measuring most physical quantities with potentially high levels of sensitivity and precision. This paper discusses recent efforts to develop a planar fiber optic acoustic sensor to quantify the low wavenumber pressure components of fluctuating pressures underneath a turbulent boundary layer (TBL). When the wavenumber characteristics of the TBL pressure fluctuations match well with the wavenumber responses of the structure of an underwater vehicle, the structure becomes easily excited and the resulting vibration can be a noise source. This vibration necessitates the need for an accurate description of the wall pressure fluctuations underneath a TBL in studying flow/structure interaction problems. The same pressure fluctuations also become unwanted noises (flow noise), which affect a hydrophone's ability to measure acoustic energy. A hydrophone capable of measuring the low wavenumber pressure components of TBL would also have reduced levels of unwanted flow-induced noises due to the high wavenumber components. Motivated by these needs of the Navy, David Taylor Research Center (DTRC) initiated the development of a planar fiber optic hydrophone with the Naval Research Laboratory (NRL).

Wall pressure fluctuations are usually characterized by their wavenumber frequency spectrum and most of the fluctuating energy lies in the convective domain. In this region, the energy in the TBL convects along the surface at the convection velocity, U_c, which is about two-thirds of the free stream velocity. While the pressure fluctuations are quite intense in this region, their scales do not match well with the structural wavelengths found for a large underwater vehicle. In the coupling between structures and low Mach number fluid flow, the subconvective, or low-wavenumber, domain becomes the dominant contributor for exciting large underwater vehicles. For an acoustic sensor, the pressure fluctuations of TBL become unwanted noise, which is commonly called flow-noise. All scales contribute to the flow noise, and each scale needs to be examined separately to determine the source; therefore, it is desirable to have a comprehensive description of the pressure statistics. Various investigators have conducted extensive analytical and experimental investigations to describe the pressure field of the TBL[1-7]. The high wavenumber components have been characterized sufficiently for practical purposes. A validated description of the low wavenumber domain, despite being an area of active experimental and analytical investigations for more than two decades, has not been attained. Studies of the coupling between structure and flow have mainly relied on semi-empirical models of the wavenumber-frequency spectrum.

In an experimental measurement, contributions by the convective domain and the vibration of the mounting structure

Figure 2:

Photograph of the planar fiber optic hydrophone.

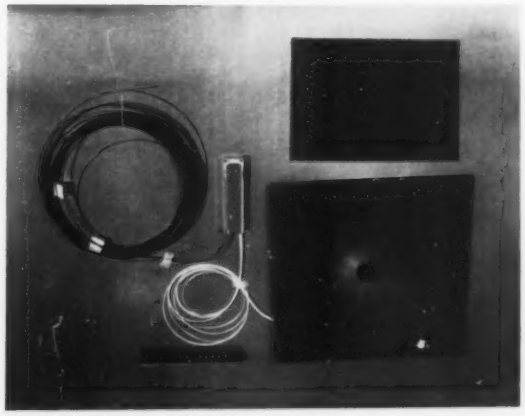

are two factors that can degrade the ability to obtain accurate low wavenumber measurements. The energy level near the convective ridge, which may be as much as 60dB higher than the low wavenumber components, makes accurate measurements difficult. This contamination by the convective domain becomes the unwanted flow noise when using hydrophones to measure acoustic energy. By providing better discrimination of high wavenumber components through area averaging of short wavelength waves, a large area hydrophone is also a hydrophone with low flow noise. Vibration of the mounting structure may also introduce unwanted noises in an experiment using large area hydrophones.

By taking advantage of the inherent geometric flexibility of fiber optic hydrophones, a large planar fiber optic hydrophone was fabricated. Unique features of the current fiber optic hydrophone design are its insensitivity to vibrational noises and its acoustical transparency. The design concept became the initial sensor design for the Low Cost (Fiber Optic) Planar Arrays (LCPA) Advanced Technology Demonstration (ATD), which aims to develop a light weight Wide Aperture Array (WAA).

A planar fiber optic hydrophone offers several practical advantages over other types of hydrophones. First, since the hydrophone and the transmission medium to the hull is fiber, it is immune to electromagnetic interference. It does not require "wet-end" electronics near the sensor to amplify the signal as in the case of conventional hydrophones. It also provides shape and size flexibility, allowing direct mounting to structures of any shape. In the case of hydrophone arrays, it may be necessary to embed the hydrophone in an elastomeric layer.

This work demonstrated that the planar fiber optic hydrophone can be a useful tool for quantifying the low wavenumber pressure components of TBL because of its encapsulating material, size, and insensitivity to vibration. Finite element models have also been developed for predicting the acoustic sensitivity of fiber optic hydrophones. Finite element analysis successfully predicted the measured sensitivity of the planar fiber optic hydrophone. Comparisons of finite element results, closed-form solutions, and experimental measurements are discussed.

Figure 3:

Acoustic response of the planar fiber optic hydrophone.

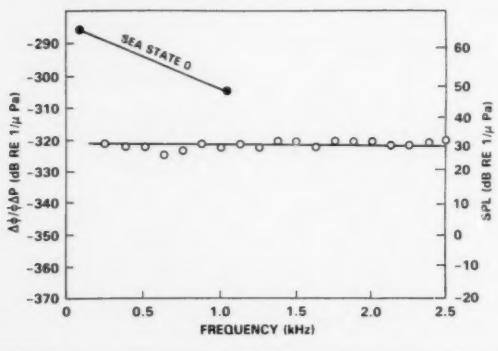

Figure 4:

Typical cross section of a finite element model for calculating the acoustic sensitivity of fiber optic hydrophone.

Planar Fiber Optic Hydrophone

Interest in developing large area planar hydrophones and obtaining an accurate description of the wavenumber-frequency spectrum of a turbulent boundary layer led DTRC to initiate the development of a large area planar fiber optic hydrophone with NRL. Fiber optic hydrophones are compatible with fiber optic communication systems. Recent developments in optical multiplexing schemes reduce the number of fibers required, which reduces the number of hull penetrations for submarine applications. The minimum detectable level of fiber optic sensors, in principle, is only limited by the quantum mechanical shot noise of the laser. At the present time, the low level noises of opto-electronics limits the performance to a level equal to conventional hydrophones. Research and development in the area of opto-electronics is rapidly improving the performance. Based on these advantages, a fiber optic hydrophone was selected over other types of hydrophones, some of which also offer size and shape flexibility, e.g., piezoelectric polymers such as polyvinylidene fluoride (PVF_2) Fabrication of the hydrophone was performed by NRL based on specifications of DTRC.

There are different methods to utilize the basic optical fiber and the transmitted light as an acoustic sensor[8]. The particular method employed most frequently in an acoustic sensor is the Mach-Zehnder all-fiber interferometer formed by the optical fibers. Figure 1 illustrates a schematic of the planar fiber optic hydrophone system. In this system, a coherent laser source emits lights at a wavelength of 800*nM* (or 1300*nM*) through the fiber. The light is then split into two parts, one

Figure 5:

Acoustic sensitivity of optical fibers encapsulated in polyurethane. ((•) represents finite element modelling).

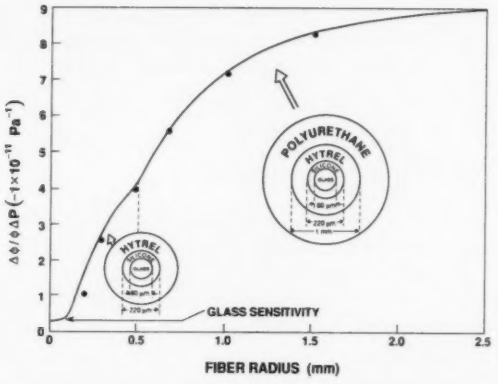

travelling through the sensing arm and another through the reference arm. In the sensing arm the fiber is made highly sensitive to acoustic pressure, while in the reference arm, without the bonding between the protective jacket (Hytrel) and the glass core, the fiber is far less sensitive. The acoustic sensitive fiber changes shape under pressure. This change in the strain within the glass core causes changes in the index of refraction of the glass core and the length of the fiber, resulting in a difference in optical path length (or phase, ϕ) between light travelling through the two arms. The phase difference ($\Delta\phi$) is directly related to the acoustic energy level. The two arms are then recombined, obtaining a phase modulated signal through the Doppler effect. The electro-optic unit fabricated for DTRC by Optech, Inc. uses a synthetic heterodyne demodulation technique for interrogating the phase modulated signal.[9]

Figure 2 depicts the planar fiber optic hydrophone developed under this work. The hydrophone consists of 30*m* of reference and 30*m* of sensing fibers wound in concentric circles to approximately 0.30*m* in diameter. These fibers are then embedded at the midplane of a polyurethane layer (6*mm* thick). Great care was taken to ensure that air bubbles were not entrapped within the polyurethane material. (Relevant properties for the fiber and polyurethane material can be found in reference 10). The unique feature of the current design is that the sensing and reference fibers are at about the same physical location. As discussed earlier, changes in path length cause the sensitivity to acoustic energy; therefore, changes in fiber length due to vibration become noise. By locating sensing and reference fibers next to each other, they are likely affected by the vibration in a similar manner. The net result is that there are minimal differences in path lengths between two fibers due to vibration (i.e., vibration cancellation). Temperature differential between two arms becomes thermal noise, which is also minimized by the close proximity of the two fibers.

The acoustic sensitivity and insertion loss of the planar fiber optic sensor were studied for 250-2500Hz and for 20-20,000Hz frequency ranges, respectively. Figure 3 shows the measured acoustic sensitivity. The sensitivity is frequency independent over the frequency range and is expressed in terms of relative optical phase shift per unit of applied acoustic pressure:

$$\frac{\Delta\phi}{\phi\Delta P} = 8.9 \times 10^{-11} Pa^{-1} = -321 dB\ re\ \mu Pa^{-1}$$

where $\phi = nkl$ is the total phase, n is index of refraction, k is the wavelength of the laser, and l is the length of the fiber. Figure 3 also shows that the planar fiber optic hydrophone is capable of measuring acoustic levels at about 15dB below Sea State 0. The insertion loss measurements for the hydrophone in an acoustic free-field demonstrated that the hydrophone is acoustically transparent. This acoustical transparency allows the potential for layering of hydrophones in an array design, offering signal processing advantages unavailable to hydrophones which are acoustically opaque. The acceleration sensitivity measurements were also made by mounting and vibrating the sensor on a very stiff honeycomb aluminum plate. The results were approximately:

$$\frac{\Delta\phi}{\phi\Delta g} = -145 dB\ re\ 1 g^{-1}$$

over the frequency range from 250Hz to 2500Hz. Combing the test results for acoustic and vibration sensitivities, one obtains the acoustic-to-acceleration sensitivity of approximately -176dB re $1g/\mu Pa$. This is approximately 15 dB less sensitive to vibration than that found for a PVF2 sensor of similar geometry. This successfully demonstrates that the cowinding scheme provides superior acceleration rejection characteristics when compared to other types of hydrophones. In the future, a planar fiber optic hydrophone will be tested for acceleration rejection with the reference fiber disconnected and using a separate reference fiber outside the hydrophone.

Figure 3 also shows the predicted sensitivity for the fiber optic hydrophone. The solid line represents the sensitivity predicted using a simplified model in which the coated fibers are assumed to be cylindrical so that closed-form solution[11] can be used. The thickness of elastomer coating was taken to be the same as the thickness of the layer, ignoring the presence of other fibers. The agreement between measured and predicted acoustic sensitivity was surprisingly good. A point of contention was the validity of this approximate model. To resolve this, a finite element analysis capability employing the WECAN finite element software of Westinghouse was developed.

The finite element model (Figure 4) was first verified by calculating the closed-form solution for an infinitely long and freely suspended fiber. The finite element results and theoretical results show excellent agreements (Figure 5), demonstrating the feasibility of using finite element modeling as a tool for fiber optic hydrophone design. The effect of different layers of coating on the acoustic sensitivity is also seen in Figure 5. The glass core is rather insensitive to acoustic pressure. The sensitivity is increased by adding the Hytrel jacket, with additional sensitivity gain through the use of elastomer coating. A finite element model is particularly valuable for more complex designs, e.g., fibers encapsulated in an inhomogeneous material such as an elastomer with varying degrees of microvoid content (gradual transition coating). The model was expanded to investigate the effects of separation distance between two embedded optical fibers on the acoustic sensitivity. Figure 6 shows the acoustic sensitivity as a function of encapsulant thickness for several different separation distances. For the cases investigated, the separation distance had no observable effects on the sensitivity. The encapsulant thickness has a greater impact on the sensitivity. Also shown are the measured sensitivity and the analytically calculated sensitivity using an effective diameter of *6mm*. The finite element result is higher than the closed-form calculation (-9 x $10^{-11} Pa^{-1}$) by about 5%. This is due to additional encapsulant material on the side of the fibers. It is expected that by modeling additional fibers, the finite element model will predict a sensitivity of about -9 x $10^{-11} Pa^{-1}$. It is important to note that results obtained from a simple finite element model and the analytical calculation do not deviate from the measured value by more than 7%, well within the experimental uncertainties. Thus, in most practical situations, fairly accurate predictions of the acoustic sensitivity of a fiber optic acoustic sensor can be obtained using the closed-form solution in which the thickness of the encapsulant layer is taken as the effective radius. However, future developments of more complex sensor concepts will require the use of finite element model developed here.

Figure 6:

Acoustic sensitivity as a function of thickness (t) of the elastomer coating for different separation distances (d) between two optical fibers (representing closed-form calculations).

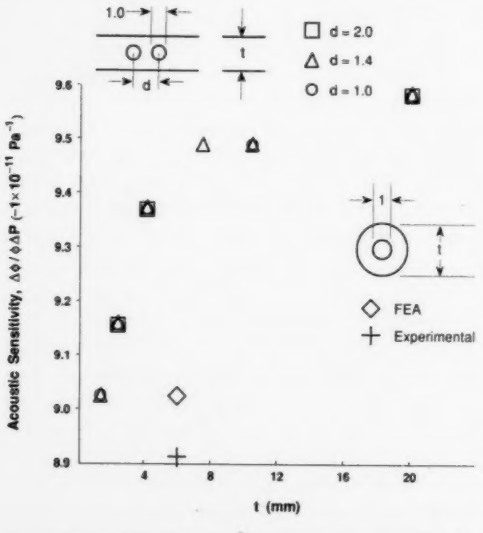

Wall Pressure Field

The wall pressure fluctuations underneath a turbulent boundary layer can be characterized by the cross-correlation of the pressures at two arbitrary points on the boundary. For a statistically homogeneous and stationary pressure field, the cross-correlation of the pressures at two points on the boundary is defined as

$$R(\xi,\tau) = < p(x,t)p(x+\xi, t+\tau) >$$

where the brackets < > denote an ensemble average, ξ is the separation distance between the two points, and τ is the time delay. The wavenumber-frequency spectrum is obtained by taking the Fourier transform of $R(\xi,\tau)$ over space and time, i.e.,

$$\Phi_p(\mathbf{k},\omega) = (2\pi)^{-3} \int_{-\infty}^{+\infty}\int_{-\infty}^{+\infty}\int_{-\infty}^{+\infty} R(\xi,\tau)\, e^{i(\mathbf{K}\cdot\xi-\omega\tau)}\, d^2\xi\, d\tau$$

where $i = \sqrt{-1}$, ω is the circular frequency, and $\mathbf{k} = (k_1, k_3)$ is the wavevector represented by the streamwise and crossflow components, k_1 and k_3, respectively. Hwang and Geib demonstrated that the wavenumber-frequency spectrum can be represented by:[2]

$$\Phi_p(\mathbf{k},\omega) = [(\phi)(\omega)/(\omega U_c)^2]G(\bar{k}_1,\bar{k}_3) \qquad (1)$$

where $G(\bar{k}_1,\bar{k}_3)$ is a normalized non-dimensional wavevector-frequency spectrum obtained from the Fourier transform of the coherence function:

$$G(\bar{k}_1,\bar{k}_3) = \frac{1}{(2\pi)^2}\int_{-\infty}^{+\infty}\int_{-\infty}^{+\infty} C(\xi_1,\xi_3)\; e^{i\,(\bar{k}_1\xi_1+\bar{k}_3\xi_3)} d\xi_1\; d\xi_3$$

where $\bar{k}_1 = U_C k_1/\omega$, $\bar{k}_3 = U_C k_3/\omega$, $\xi_1 = \omega\xi_1/U_C$, and ξ_3 $\omega\xi_3/U_C$. The general belief is that the wavenumber-frequency spectrum obtained from the Fourier transformation of the Corcos-type (exponential decay) coherence function, as shown above, is only useful for determining structural response when the principal sources of excitation are the wavenumber components near hydrodynamic coincidence. For the purpose of extending the applicability to the sub-convective (or the low-wavenumber) as well as the acoustic

Figure 7:

Non-dimensionalized wavenumber-frequency spectrum of turbulent boundary layer.

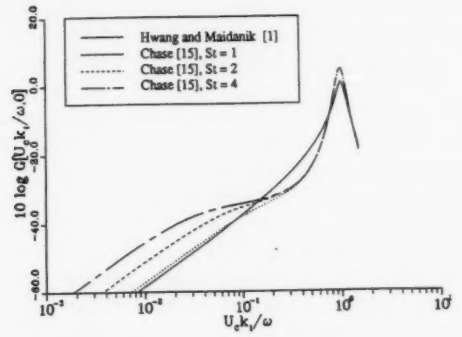

wavenumber domains, many theoretically derived and empirically fitted spectral models have been developed and published in recent years[12-21]. However, none of the models have been convincingly validated or ascertained to predict the low-wavenumber portion of the spectrum. Hwang and Maidanik[1] proposed a rather simple modified Corcos-type spectrum given by

$$G(\bar{k}_1,\bar{k}_3) \equiv \frac{1}{\pi^2(1+\bar{k}_3^2)} \begin{cases} \dfrac{0.145\bar{k}_1^2}{0.012+(\bar{k}_1-1)^2}, & -0.2 \le \bar{k}_1 \le 1 \\ \dfrac{0.145(2-\bar{k}_1)^2}{0.012+(\bar{k}_1-1)^2}, & 1 \le \bar{k}_1 \le 2 \\ 0, & \bar{k}_1 < -0.2 \text{ or } \bar{k}_1 > 2 \end{cases} \quad (2)$$

which, because of its conservative estimation of low wavenumber and acoustic regions, is particularly useful in this discussion. Hwang and Shang employed the same model for studying the effect of transition on the coupling of structure and fluid flow.[3] Figure 7 shows the wavenumber frequency spectrum for zero cross-flow wavenumber and at a fixed frequency in terms of the streamwise wavenumber as given by equation 2 and Chase for several different Strouhal numbers.[15] The shape of the wavenumber spectrum near the convective ridge is rather well established by cross spectral density measurements, but the low wavenumber region (say, $U_c k_1/\omega < 0.1$) remains largely conjectural. Low wavenumber measurements are typically contaminated by the convective ridge and acoustic field in the high and low wavenumber regions, respectively. A clamped flat plate type of spatial filter exhibits the most superior performance at rejecting high-wavenumber components. A transducer with uniform response act like a free plate, which requires a large area to average out the high wavenumber components. Unwanted contamination from the acoustic field may be rejected using hydrophone arrays. Past experiments have either used arrays or plate-like structures for the rejection of unwanted fields. The unique features of fiber optic hydrophones allow the construction of a large area hydrophone in a linear array, simultaneously offering the functionality of free plate-like spatial filtering (for the high wavenumber rejection) and array-like beamforming (for acoustic wavenumber rejection).

In actual measurement, the properties of the measuring device must be taken into consideration. Several factors affect the measurement of the wavenumber-frequency spectrum, $\Phi_p(k,\omega)$, and the frequency spectrum, $\Phi(\omega)$, including the finite size and shape of the transducer, the elastomeric coating material covering the transducer, and the frequency response of the instrumentation. In addition, the hydrophones may be arranged in linear array whose response can be used to obtain different measurements. Therefore, instead of $\Phi_p(k,\omega)$, one obtains

$$\Phi_M(\boldsymbol{k},\omega) = |S(\boldsymbol{k},\omega)|^2 T(\boldsymbol{k},\omega)|A(\boldsymbol{k})|^2 |H(\omega)|^2 \Phi_p(\boldsymbol{k},\omega) \quad (3)$$

where $\Phi_M(\mathbf{k},\omega)$ is the measured wavenumber-frequency spectrum, $|S(\mathbf{k},\omega)|^2$ is the wavenumber sensitivity function of the hydrophone. $T(k,\omega)$ represents the transmissibility, or the filtering property, of the elastomeric layer, $|A(\mathbf{k})|^2$ represents the array response, and $|H(\omega)|^2$ is the frequency filtering by the measuring instruments. Substituting equation (1) into equation(3), one obtains the following expression

$$\Phi_M(\boldsymbol{k},\omega) =$$

$$|S(\boldsymbol{k},\omega)|^2 T(\boldsymbol{k},\omega)|A(\boldsymbol{k})|^2 |H(\omega)|^2 [\phi(\omega)/(\omega U_c)^2] G(\bar{k}_1,\bar{k}_3)$$

Figure 8:

Wavenumber sensitivity function for circular hydrophones.

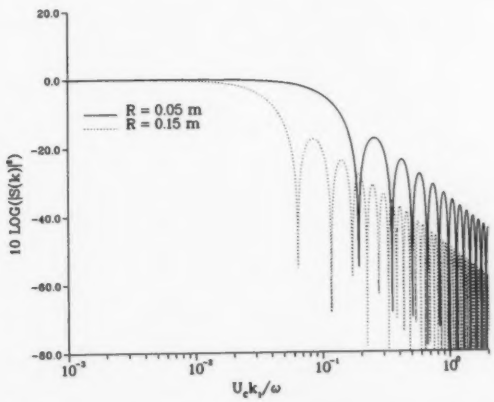

It is generally accepted that the response function for a hydrophone is independent of frequency, i.e. $|S(\mathbf{k},\omega)|^2 = |S(\mathbf{k})|^2$.

In typical measurements, frequency filters are readily available and only terms that have wavenumber dependence are of interest. The remaining discussions will focus on the role of each parameter, particularly as applied to the fiber optic hydrophone described in the previous section. Furthermore, available data indicate that $\Phi_p(k,\omega)$ is a slow varying function of k_3 and the remaining discussions will center on the more interesting dependence of $\Phi_p(k,\omega)$ on k_1 and ω.

In the near future, experiments for determining the flow noise characteristics of the hydrophone and for measuring the TBL wavenumber-frequency spectrum will be carried out in a water tunnel or on buoyancy-propelled model scale submarines available at the Acoustic Research Detachment of DTRC, Bayview, Idaho. These model scale submarines, which have been used extensively by the Navy for research and development related to flow generated noises and flow structure interaction, offer the advantage that they do not have any mechanical devices, allowing isolation of noises caused by the turbulent boundary layer. In these experiments, a model scale submarine is lowered to about 300*m* deep in a fresh water lake and released to rise to the surface under its own buoyancy.

Wavevector Filter Technique

In order to decompose the pressure field into its spatial and temporal components as represented by the wavenumber and frequency variables, an instrument that senses energy in a frequency band centered at some frequency ω_o and at some wavenumber $k_{1,0}$ is necessary. Since frequency filters are readily available, the problem becomes one of involving development of a spatial filter with a known response function. If the bandwidths are sufficiently small, the spectral density at ω_o and $k_{1,0}$ can be obtained. A spatial filter designed specifically to have this type of measurement is commonly called a wavevector filter.[4]

In principle, any device that responds to pressure can be a wavevector filter. Either flush mounted hydrophones or structures can be used to perform the spatial filtering of the signal. In practical measurement, the output is passed through a frequency filter, which performs the frequency filtering of the signal. Spatial and temporal Fourier transforms are then taken to obtain the spectral density at ω_o and $k_{1,0}$.

For a circular hydrophone of radius R, the wavenumber sensitivity function is $|S(\mathbf{k})|^2 = |[2J_1(kR)/kR]^2$ where $k=(k_1^2 + k_3^2)^{\frac{1}{2}}$ and J_1 is the Bessel function. Figure 8 displays the wavenumber sensitivity function for circular hydrophones of two different sizes as a function of a normalized wavenumber. The sensing surface was assumed to have uniform sensitivity across the sensing area. Thus a hydrophone with larger area is better at filtering the high wavenumber components of TBL because of the area averaging of pressure fluctuations of short wavelengths. The roll-off at high wavenumber can be further enhanced by appropriate shading of the sensitivity across the surface.

Figure 9:

Wavenumber sensitivity function for a linear array in the sum (.....) and difference (———) modes.

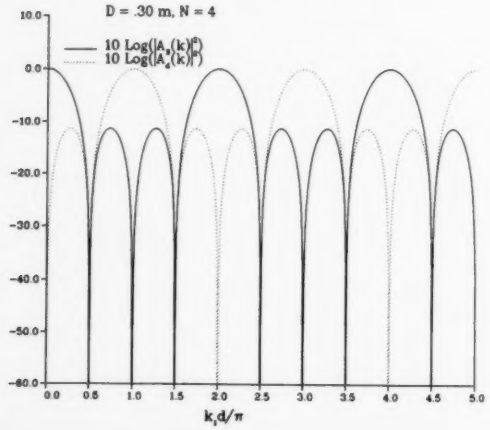

Figure 10:

Effect of size and polyurethane encapsulant of planar fiber optic hydrophone on the wavenumber spectrum of turbulent boundary layer.

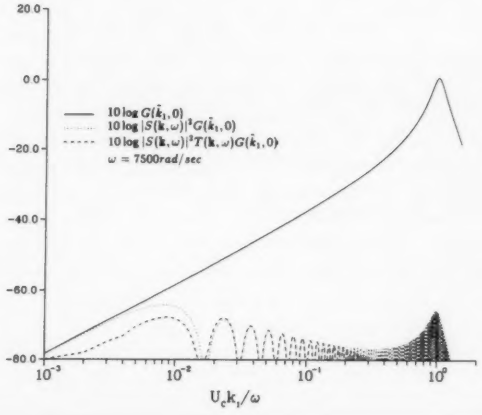

Figure 11:

The wavenumber spectrum of turbulent boundary layer as measured by a four-element array of planar fiber optic hydrophones.

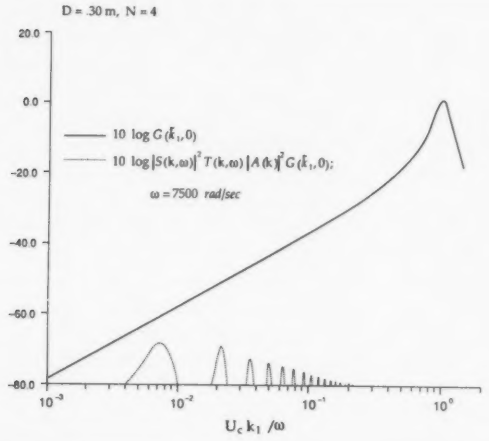

Linear Array

Several parameters come into consideration when using a linear array as a wavevector filter. An excellent discussion on this subject can be found in Geib.[4] Here, only parameters that are relevant in designing a linear array consisting of the planar fiber optic hydrophones are discussed. These parameters include the center-to-center spacing of hydrophones, d, method of summing hydrophone outputs, and number of hydrophones, N.

When an array is made up of a number of equally spaced hydrophones with center-to-center separation d, the equation governing the array gain is the same as for diffraction gratings. Major response lobes occur at multiple of $\pm k_1 d/\pi$. The number and magnitude of minor lobes, which occur between the major lobes, are increasing and decreasing function of the number of hydrophone, respectively. The array gain for the sum and difference modes of a collinear array in the flow direction are given as[7]

$$A_s(k_1) = \frac{\sin\frac{1}{2}Nk_1d}{N\sin\frac{1}{2}k_1d}\, e^{i(N-1)kd/2}$$

and

$$A_s(k_1) = \frac{\sin\left[\frac{1}{2}N(k_1d-\pi)\right]}{N\sin\left[\frac{1}{2}(k_1d-\pi)\right]}$$

respectively. In a difference mode, outputs from the elements are summed alternately; in a sum mode outputs from the elements are summed together. Figure 9 shows the array gain for sum and difference modes of a four-element array as a function of normalized wavenumber $k_{1d/\pi}$. For removing the facility acoustic noises, the difference mode is more useful for measuring the low wavenumber components of TBL. Additional reduction of grating lobes can be accomplished through spatial and amplitude shading techniques by varying separation distance d and assigning different amplitude weights, respectively. In addition, the array can be steered by adding time delays in the array output.

Effects of Encapsulating Material

For the fiber optic hydrophone shown in Figure 2, optical fibers are encapsulated in an polyurethane material (Uralite 3140). As discussed earlier, this additional coating serves to increase the acoustic sensitivity of the fiber optic hydrophone. The polyurethane layer provides an additional benefit, which is filtering of high wavenumber components of the TBL. This means that the elastomer layer also acts as an outer decoupler, which precludes the passage of waves whose wave speeds are less than the characteristic wave speed of the elastomer. Since wavenumbers are inversely proportional to wave speeds, the outer decoupler is also considered to be a low-pass wavenumber filter. Hwang and Kim provide a comprehensive analytical description for wave transmission through a multi-layered system by considering the transmission and reflection of

Figure 12:

Conceptual schematic of a fiber optic hydrophone embedded within a gradual transition coating.

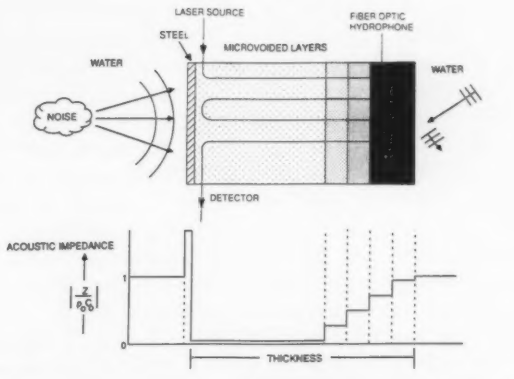

waves at each interface and obtained good agreement between predicted and measured pressure levels for an embedded array of PZT hydrophones.[17]. Their method was used in this study for calculating the transmissibility through the layer of encapsulant material of the fiber optic hydrophone, which is directly mounted on the hull of a model scale submarine.

Numerical Examples

Parameters that are pertinent to the current fiber optic hydrophone design are examined to demonstrate the feasibility of quantifying the low wavenumber domain. Figure 10 displays the wavenumber sensitivity function of the fiber optic hydrophone, $|S(k)|^2$, the normalized wavenumber frequency spectrum, $G(k_1, 0)$, and their product, $G(k_1, 0)|S(k)|^2$. Relevant flow parameters are $U_c = 5m/sec$, $\omega = 7500\ rad/sec$. The hydrophone array is mounted on a $1.5cm$ thick steel plate with both sides exposed to water. The levels near the convective ridge, which is due to waves of short wavelengths, are suppressed by the area averaging characteristics. However, the levels are still of about the same order of magnitude as the low wavenumber components. As mentioned earlier, the polyurethane used to encapsulate the optical fibers provides additional attenuation of high wavenumber components. The effect of transmissibility $T(k, \omega)$ is added to the effects of area averaging, and the net result, $G(k_1, 0)|S(k)|^2 T(k,\omega)$, is also displayed in Figure 10. The spectral peak at the convective wavenumber is substantially reduced by the filtering action of the elastomer. The resonance seen in Figure 10 is associated with the plate resonance. A linear array can provide suitable array gain so that additional suppression of unwanted signals can be attained. In experiments to be conducted on scale model submarines, a four-element array can be appropriately placed on the hull. An array allows many possibilities for data processing. For illustrative purposes, a four element array operating in the difference mode is shown in Figure 11. As one can readily observe from the levels of $G(k_1, 0)|S(k)|^2 T(k,\omega) A(k,\omega)|^2$, the contamination due to acoustic components is substantially reduced. In the example, all the aliasing lobes are more than 3dB below the main response lobe. The levels of these side lobes may actually be lower than what are shown. The Hwang and Maidanik model conservatively estimates the low wavenumber domain with a k_1^2 dependence and there are evidences to suggest that the wavenumber-frequency spectrum in the low wavenumber domain is wavenumber white.[15] The levels of the side lobes are not sufficiently reduced to allow direct measurements of TBL spectral levels in the low wavenumber domain, which means that spatial and amplitude shading techniques are required to further suppress the side lobes. A treatment of these techniques is beyond the scope of the present discussion.

Concluding Remarks

A planar fiber optic hydrophone based on the Mach-Zehnder all-fiber interferometer has been successfully developed. The acoustic sensitivity of the hydrophone was the best among planar fiber optic hydrophones. The hydrophone has low flow noise through area averaging, making it ideally suited for underwater applications. The hydrophone has achieved low sensitivity to vibration by winding the sensing and reference fibers next to each other. This winding is important for applications in which the basic supporting structure is vibrating. In an array application, this insensitivity to vibration may allow direct mounting of the hydrophone to the hull of underwater vehicles, potentially reducing the weight by eliminating some hardware. Acoustical transparency of the fiber optic hydrophone may allow an array designer to have multiple layers of the hydrophone to gain additional signal processing advantages or place the array in front other conventional hydrophones. The design concept reported in this paper was the basis for the Low Cost (Fiber Optic) Planar Array (LCPA) Advanced Technology Demonstration (ATD) program. The program, which is scheduled to commence in Fiscal Year 1991, is intended to develop a light weight wide aperture array.

The pressure fluctuations underneath a turbulent boundary layer are responsible for the coupling between structures and fluid flow; therefore, it is important to have a validated description of the wavenumber-frequency spectrum of the turbulent boundary layer. The part of the spectrum that is mostly responsible for noise producing flow-structure interaction is the subconvective, or low-wavenumber, domain, which, despite being an area of active experimental and analytical investigations for more than two decades, can not be accurately described. Studies of the coupling between structures and flow have relied on semi-empirical models of the wavenumber-frequency spectrum. Numerical examples (Figures 10 and 11) show that the planar fiber optic hydrophone possesses potential for quantifying flow noises. Additional work is required to explore amplitude and spatial shading techniques so that further reduction of side lobes can be achieved.

Future work will attempt to take advantage of the uniqueness of the transduction method of fiber optic sensors. The fiber optic hydrophone described in this work does not measure pressure directly, rather the pressure causes deformation of the material, which, in turn, produces phase differences between light travelling through the two arms of the interferometer. In the case of a pressure release material, where the pressure is minimal, a traditional hydrophone does not function satisfactorily. A suitably designed fiber optic hydrophone can be made to indirectly, but accurately, measure the acoustic pressure as the material deformation produces strain within the fiber. Figure 12 shows a possible design of such a fiber optic hydrophone embedded within a gradual transition coating.

The finite element modeling capability described here will be used to explore different design concepts.

Biographies

Paul Shang received his Ph.D. in mechanical engineering from Rutgers University in 1984. He has been with the David Taylor Research Center for seven years and is the head of the Flow Noise Branch.

Paul Zoccola earned his BSE from the University of Pennsylvania in 1984 and his MME from Catholic University in 1989. He has been a mechanical engineer in the Flow Noise Branch at the David Taylor Research Center since 1985.

Stanley Fisher graduated from the University of Maryland in 1966 with a bachelors degree in physics. He has worked at the David Taylor Research Center since 1967 and is currently the Director of Research Operations in the Acoustic Technology Division.

Yun-Fan Hwang received his Ph.D. in acoustics from the Pennsylvania State University in 1975. He has been with the David Taylor Research Center since 1978 and is a Senior Scientist in the Acoustic Technology Division.

References

1. Y.F. Hwang and G. Maidanik, A wavenumber analysis of the coupling of a structural mode and flow turbulence, to be published in *Journal of Sound and Vibration*, 1990.
2. Y.F. Hwang and F.E. Geib, Estimation of the wavevector-frequency spectrum of turbulent boundary layer wall pressure by multiple linear regression, *ASME Journal of Vibration, Stress, and Reliability in Design*, **106**, pp. 334-342, 1984.
3. Y.F. Hwang and P.C. Shang, Effects of laminar-turbulence transition on the coupling of structural modes and fluid flow, in Flow-induced Noise due to laminar-turbulence transition process, Eds: T.M. Farabee, *et al.*, ASME Winter Annual Meeting, San Francisco, California, Dec., 1989.
4. F.E. Geib, Jr. Practical requirements of turbulent boundary layer forcing function measurements as wave-vector filters, Symposium on the Flow-induced Vibrations, **5**, Turbulence-induced Noise and Vibration of Rigid and Compliant Surfaces, ASME Winter Annual Meeting, Dec., 1984.
5. H.M. Helal, M.J. Casarella, and T.M. Farabee, An application of Noise Cancellation techniques to the measurement of wall pressure fluctuations in a wind tunnel, in Flow-induced Noise due to laminar-turbulence transition process, Eds: T.M. Farabee, *et al.*, ASME Winter Annual Meeting, San Francisco, California, Dec., 1989.
6. P. Leehey, Structural Excitation by a Turbulent Boundary Layer: an Overview, *Transaction of ASME*, Vol. 110, pp. 220-225, 1988.
7. W.K. Blake, *Mechanics of Flow-Induced Sound and Vibration, Vol,* **I & II, Academic Press, 1986.**
8. T.G. Giallorenzi, *et al.*, Optical fiber sensing technology, *IEEE J. Quantum Electron.* **QE-18**, pp. 626-666, 1982.
9. A. Dandridge, *et al.*, Homodyne demodulation scheme for fiber optic sensors using phase generated carrier, *IEEE Journal of Quantum Electronics*, **QE-18**, pp. 1647-1653, 1982.
10. N. Lagakos, *et al.*, Planar Flexible Fiber Optic Acoustic Sensor, *Optic Letters*, **13**, pp. 788-783, 1988.
11. B. Budiansky, *et al.*, Pressure sensitivity of a clad optical fiber, *Applied Optics*, **18**, pp. 4085-4088, 1979.
12. G.M. Corcos, Resolution of pressure in turbulence, *Journal of the Acoustical Society of America*, **35**, 192-199, 1963.
13. D.M. Chase, Modeling the wavevector-frequency spectrum of turbulent boundary layer wall pressure, *Journal of Sound and Vibration* **70**, 29-67, 1980.
14. J.E. Ffowcs-Williams, Boundary layer pressure and Corcos model: A development to incorporate low-wavenumber constraints, *Journal of Fluid Mechanics* **125**, 9-25, 1982.
15. D.M. Chase, The character of the turbulent wall pressure spectrum at subconvective wavenumbers and a suggested comprehensive model, *Journal of Sound and Vibration* **112**, 125-147, 1987.
16. J.M. Witting, A spectral model of pressure fluctuations at a rigid wall bounding an incompressible fluid, based on turbulent structures in the boundary layer, *Noise Control Engr. Journal* **26**, 28-43, 1986.
17. Y.F. Hwang and M. Kim, Prediction of flow-induced noise in a multi-layer system, Symposium on Underwater Acoustics, David Taylor Naval Ship Research and Development Center, 1983.
18. P.W. Jameson, Measurement of low wavenumber component of turbulent boundary layer wall pressure spectrum, *Bolt, Beranek and Newman Report No. 1937*, 1970.
19. T.M. Farabee and F.E. Geib, Jr., Measurement of boundary layer pressure fields with an array of pressure transducers in a subsonic flow, *Proceedings of the 6th Int. Cong. on Instrumentation in Aerospace Simulation Facilities, Ottawa, Canada*, 1975.
20. F.E. Geib and T.M. Farabee, Measurement of boundary layer pressure fluctuations at low wavenumber on smooth and rough walls, *David Taylor Naval Ship R & D Center Report No. 84-05*, 1985.
21. N.C. Martin and P. Leehey, Low wavenumber wall pressure measurements using a rectangular membrane as a spatial filter, *Journal of Sound and Vibration* **52** 95-120, 1977.

Research Notes

Two Major Oceanographic Instrument Programs to Form Global Grid for Circulation Experiments

Marine scientists will have access to direct, real-time information on ocean currents and overlying weather conditions around the world for the first time as part of two major research programs of the Scripps Institution of Oceanography, University of California, San Diego.

Reporting at the American Geophysical Union's Fall Meeting in San Francisco, Calif., Drs. Russ E. Davis and Pearn P. Niiler will describe ocean monitoring programs that employ hundreds of newly designed, drifting ocean instruments to be tracked by satellites for global ocean data-gathering. Some drifters are in place in the Atlantic and Pacific oceans now, and by the mid 1990s these devices will form a worldwide grid over the oceans. The instruments were developed at Scripps with funding by the Office of Naval Research.

According to the scientists, the programs will provide data needed for studying and forecasting large-scale ocean and atmospheric conditions and for determining how the ocean will respond to future global climate changes. Such information also is important for weather forecasting and fisheries questions.

Both Scripps Institution programs are integral parts of United States participation in the International World Ocean Circulation Experiment (WOCE), a five-year program sponsored by UNESCO's World Climate Research Program. A primary goal of WOCE is understanding the general circulation of the global ocean well enough to enable modeling of its present state and to make predictions of long-term oceanic changes.

The Scripps scientists will be providing new data sets of highly reliable measurements of temperature and atmospheric pressure over the oceans and of ocean water circulation from the surface to depths as great as 2,000 meters (6,000 feet). Subsurface data collection is accomplished by using autonomous, deep-floating instruments that periodically rise to the surface to transmit their measurements. Surface measurements involve large deployments of uniquely designed drifters that relay highly accurate ocean-atmosphere information.

"Today there is great interest in how the ocean participates in the atmospheric heat budget of the world and the question of how carbon dioxide is mixed into the oceans from the atmosphere. Measuring large-scale ocean circulation is critical to understanding these complicated questions," said Davis, a Scripps Institution professor of physical oceanography. "Floating instruments are the only practical way to obtain continual observations over large areas of the ocean where there is little or no research ship activity or commercial ship traffic. These two efforts are the first programs to directly measure global patterns of ocean circulation at surface and subsurface levels."

Davis deployed his first eight operational deep-water floats in January 1990 in the Southern Ocean's Drake Passage, where they continue to report monthly their locations for a circumpolar ocean circulation investigation. During the next four years, his research team plan to place some 350 floats in the Pacific Ocean for WOCE studies.

Niiler is the director of a program in which 200 drifters are out now in the tropical Pacific as part of a pilot program sponsored by the Tropical Ocean Global Atmosphere (TOGA) program. During 1991, 200 more instruments will be placed in the Pacific from South American to Alaska as part of his surface circulation program for WOCE. Eight Pacific Rim Countries will participate in the program. In the next four years, the effort will expand into the Atlantic, Indian, and Southern oceans for a total of 1,100 to 1,300 drifters. The drifters measure sea-surface velocity, temperature, and barometric pressure on ocean basin scales and over seasonal time scales, data required by both WOCE and TOGA programs.

"We want to redraw the water motion charts of world's oceans," said Niiler, a Scripps Institution professor of applied mechanics. "We will be providing information from which maps of global surface currents and their variances can be constructed. These observations will be used to test global models of ocean circulation and to improve the accuracy of measurements made by remote sensing instruments on satellites.

Niiler's surface drifters are from an ocean-observing system similar to the well-developed network of land-based weather stations that have provided basic meteorological information since the 1940s. The data they collect is relayed to NOAA-N series ARGOS satellites and available to scientists through the National Oceanic and Atmospheric Administration's Atlantic Oceanographic Meteorological Laboratory's Drifter Data Center, Miami, Fla.

Each drifter consists of a small, spherical instrument package that floats on the surface connected by wire to a nylon, tube-shaped sock, about 18 feet long and 3 feet in diameter

that hangs below the sea-surface about 45 feet. This design keeps the instrument stable in the water column and eliminates the effects of overlying winds. It will follow water motions to an accuracy of 1/2 mile per day, a 25-fold improvement over how currents are measured by recording the drift of ships. Such precise measurements of the water movement have not been available previously, according to Niiler.

Davis's deployments of subsurface floats will allow direct observation of deeper ocean currents on a global basis, an important element of the WOCE program. The small subsurface current-following floats periodically rise to the surface where they are located by the same ARGOS satellites as the surface drifters.

"Unlike currents at surface, which are directly influenced by the wind, subsurface currents are generally slower and less turbulent," Davis said. "At the depths we will be measuring for WOCE, about 3,000 to 4,000 feet beneath the surface, the water motion is typically a few hundred feet per day. By averaging together many different floats in one area and then drawing maps of velocity fields, we can use the water density observations in WOCE to calculate particle motion up and down the water column."

Before deployment, the instrument's float is ballasted to be neutrally buoyant at the desired depth. It sinks and stays at great depths for about a month. A preprogrammed commend from a microcomputer controller triggers a hydraulic system that increases the float volume and causes it to surface. It remains on the surface for 24 hours, during which time an ARGOS transmitter is activated so that the float may be located by satellite. The cycle then begins again. The instruments are housed in a 6.5-inch diameter aluminum tube, 6 feet long, and weighing 50 pounds.

DEPARTMENT OF THE NAVY
OFFICE OF NAVAL RESEARCH
ARLINGTON, VA 22217

OFFICIAL BUSINESS
PENALTY FOR PRIVATE USE, $300